Site-selective generation of lanthanoid binding sites on proteins using 4-fluoro-2,6-dicyanopyridine

Sreelakshmi Mekkattu Tharayil,[1] Mithun C. Mahawaththa,[2] Akiva Feintuch,[3] Ansis Maleckis,[4] Sven Ullrich,[1] Richard Morewood,[1] Michael J. Maxwell,[2] Thomas Huber,[1] Christoph Nitsche,[1] Daniella Goldfarb,[3] Gottfried Otting[2]

[1] Research School of Chemistry, Australian National University, Canberra, ACT 2601, Australia

[2] ARC Centre of Excellence for Innovations in Peptide & Protein Science, Research School of Chemistry, Australian National University, Canberra, ACT 2601, Australia

[3] Department of Chemical Physics, Weizmann Institute of Science, Rehovot 76100, Israel

[4] Latvian Institute of Organic Synthesis, Aizkraukles 21, LV-1006, Riga, Latvia

Correspondence to: Gottfried Otting (gottfried.otting@anu.edu.au)

Abstract. The paramagnetism of a lanthanoid tag site-specifically installed on a protein provides a rich source of structural information accessible by nuclear magnetic resonance (NMR) and electron paramagnetic resonance (EPR) spectroscopy. Here we report a lanthanoid tag that reacts selectively with cysteine or selenocysteine with formation of a (seleno)thioether bond and a short tether between lanthanoid ion and protein backbone. The tag is assembled on the protein in three steps, comprising (i) reaction with 4-fluoro-2,6-dicyanopyridine (FDCP), (ii) reaction of the cyano groups with α-cysteine, penicillamine or β-cysteine to complete the lanthanide chelating moiety and (iii) titration with a lanthanoid ion. FDCP reacts much faster with selenocysteine than cysteine, opening a route for selective tagging in the presence of solvent-exposed cysteine residues. Loaded with Tb^{3+} and Tm^{3+} ions, pseudocontact shifts were observed in protein NMR spectra, confirming that the tag delivers good immobilisation of the lanthanoid ion relative to the protein, which was also manifested in residual dipolar couplings. Completion of the tag with different 1,2-amino thiol compounds resulted in different magnetic susceptibility tensors. In addition, the tag proved suitable for measuring distance distributions in double electron–electron resonance experiments after titration with Gd^{3+} ions.

1 Introduction

Site-specific labelling of a protein with a paramagnetic lanthanoid ion opens many possibilities to investigate the structure of the protein by NMR and EPR spectroscopy. The presence of a paramagnetic lanthanoid ion produces long-range paramagnetic effects that can be observed by NMR spectroscopy. Among these, pseudocontact shifts (PCS) are particularly straightforward to measure and useful for the structural analysis of proteins (Otting, 2010). Using EPR spectroscopy, tags with Gd^{3+} ions have proven highly attractive for measuring nanometre scale distances by double-electron–electron resonance (DEER) experiments

Formatted: Superscript

Deleted: characterisation

(Giannoulis et al., 2021). The outstanding utility of these experiments has triggered the development of numerous reagents and strategies for site-specific attachment of lanthanoid ions to proteins and other biological macromolecules (Miao et al., 2022).

To create useful structural information, the ideal lanthanoid binding site should fulfil several criteria. (i) The lanthanoid ion must be held in a defined position relative to the protein to minimize averaging of PCSs and provide accurate distance information in DEER experiments. This is best achieved by tags that are tied to the protein via a short and rigid linker that nonetheless must not affect the structure of the protein. (ii) The binding site must be site-specific. Most lanthanoid tags are designed for covalent bond formation of a synthetic lanthanoid complex with cysteine thiol groups, but specific attachment to a genetically encoded non-canonical amino acid would be even more attractive. (iii) The tag should be straightforward to synthesize to save costs and effort. (iv) The metal must bind to the tag with sufficient affinity to prevent free metal ions from binding to the protein elsewhere.

In principle, these criteria could be fulfilled by a non-canonical amino acid designed for directly binding a lanthanoid ion and amenable to incorporation into the polypeptide chain in response to a stop codon. The amino acid 2-amino-3-(8-hydroxyquinolin-3-yl) propanoic acid has been genetically encoded for this purpose, but its presence in proteins leads to quantitative precipitation upon titration with lanthanide ions (Jones et al., 2010). Phosphoserine is another genetically encoded amino acid capable of metal binding and has successfully been used, in conjunction with another negatively charged amino acid, to generate lanthanoid binding sites in proteins (Mekkattu Tharayil et al., 2021). Unfortunately, the high concentration of negative charges compromises protein stability and expression yields, limiting the approach to highly stable proteins only.

If a longer tether between the protein backbone and the gadolinium ion can be accepted, the non-canonical amino acid *p*-azidophenylalanine can be installed in the target protein site-selectively, followed by covalent attachment of a gadolinium complex in a Cu^{+}-catalysed click reaction (Abdelkader et al., 2015). Unfortunately, many proteins precipitate upon exposure to the Cu^{+} catalyst and the synthesis of suitable gadolinium complexes is demanding.

The present work sought to identify a lanthanoid tag that fulfils the criteria of rigidity, affordability and selectivity for the non-canonical amino acid selenocysteine, which can be incorporated into proteins site-selectively by using a photocaged precursor (Welegedara et al., 2018). The tagging approach uses a strategy of chemical assembly on the target protein, which is based on recently introduced conjugation chemistry, where a cyano-pyridine is ligated with a 1,2-aminothiol under biocompatible conditions (Nitsche et al., 2019). The tag assembly starts by reacting FDCP with cysteine or selenocysteine in a nucleophilic substitution reaction. In the next step, the dicyanopyridine (DCP) moiety is reacted with two molecules of cysteine, penicillamine or β-cysteine to complete the lanthanide binding motif on the protein (Fig. 1).

The capacity to assemble different tags from readily accessible building blocks is of particular interest for protein structure elucidation. Recent results showed that the installation of four or more tags at the same protein site enable high-resolution structure determinations at selected sites from PCSs only, provided that the tags generate magnetic susceptibility anisotropy tensors of different orientation (Orton et al., 2022).

In the following, we report on the selectivity of the approach, reaction yields and performance in PCS and DEER measurements.

2 Experimental procedures

2.1 Expression vector construction

Expression vectors were as published previously (Liepinsh et al., 2001; Guignard et al., 2002; Potapov et al., 2010; Yagi et al., 2011; Welegedara et al., 2017 and 2021; Johansen-Leete et al., 2022) or prepared specifically for the present work (Table S4) by cloning the gene between the *Nde*I and *Eco*RI sites of the T7 vector pETMCSI (Neylon et al., 2000). The final plasmids were constructed using a reliable and quick version of sequence and ligation independent cloning (RQ-SLIC) and mutagenesis experiments were conducted by QuikChange. Both protocols relied on a mutant T4 DNA polymerase and were used as described by Qi and Otting (2019).

2.1 Protein expression

Samples of nine different proteins were produced. The proteins were the *E. coli* peptidyl-prolyl *cis-trans* isomerase PpiB, the N-terminal domain of *P. falciparum* Hsp90, rat ERp29 and its cysteine mutants S114C/C157S and G147C/C157S, the SARS-2 main protease, the T237C/T345C mutant of the maltose binding protein (MBP), the Q32C cysteine mutant of the B1 immunoglobulin-binding domain of streptococcal protein G (GB1), and the intracellular domain of the p75 neurotrophin receptor ($p75^{NTR}$). All expression plasmids were pETMCSI plasmids. All proteins were expressed in *E. coli* BL21 DE3 cells transformed with the requisite plasmid. Expressions in unlabelled rich media used 1 L of cell-culture grown in LB medium with 50 µM spectinomycin and 50 µM kanamycin at 37 °C until the OD_{600} value reached 0.6–0.8. Expression was induced with 1 mM IPTG. Afterwards, the culture was grown at room temperature overnight. ^{15}N labelling was achieved using a modified protocol developed for a fermenter (Klopp et al., 2018). Initially cells were inoculated in 25 mL ^{15}N minimal medium (6.8 g/L KH_2PO_4, 7.1 g/L Na_2HPO_4, 0.71 g/L Na_2SO_4, 2.0 mL/L 1 M $MgCl_2$, 18 g/L glucose, 2.6 g/L $^{15}NH_4Cl$, 0.2 mL/L trace metal mixture as recommended by Klopp et al.) and grown overnight at 37 °C shaking at 220 rpm. The overnight culture was inoculated into 0.5 L ^{15}N minimal fermenter medium in a Labfors 5 fermenter (Infors, Bottmingen, Switzerland) and grown until OD_{600} reached 12–13, then 9 g glucose and 1.3 g of $^{15}NH_4Cl$ were added and expression induced with 1 mM IPTG. After induction, the cultures were grown at 18 °C overnight for protein expression.

The cells were harvested by centrifugation at 5,000 *g* for 15 minutes and lysed by passing twice through a Emulsiflex-C5 Homogenizer (Avestin, Canada). The lysate was centrifuged at 13,000 *g* for 1 h and the filtered supernatant loaded onto a 5 mL Ni-NTA column (HisTrap FF column; GE Healthcare, USA) equilibrated with binding buffer (50 mM Tris-HCl, pH 7.5, 300 mM NaCl, 5 % glycerol). The protein was eluted with elution buffer (binding buffer containing, in addition, 300 mM imidazole) and the fractions were analysed by 12 % SDS-PAGE. Subsequently, for the proteins used for NMR measurements, the His_6-tag was removed by digestion overnight at 4 °C, using TEV protease added in 100-fold excess in buffer containing 50 mM Tris-HCl, pH 8.0, 300 mM NaCl and 1 mM β-mercaptoethanol.

Formatted: Don't adjust space between Latin and Asian text, Don't adjust space between Asian text and numbers

Formatted: Font: Not Italic

Formatted: Font: Not Italic

Deleted: , where

Deleted: b

Deleted: (

Deleted: et al.

Deleted: ,

Formatted: Font:

Deleted: were produced

Deleted: maltodextrin

Deleted: Standard

Deleted: e

Calmodulin K148U and MBP T237U/T345U (where U stands for selenocysteine) were produced by cell-free protein synthesis following a published protocol (Welegedara et al., 2021). In the cell-free protein synthesis reaction, cysteine was replaced by selenocysteine and 10 mM dithiothreitol (DTT) were added to keep selenocysteine in the reduced state. Protein purifications used a 1 mL Co-NTA column (His GraviTrap TALON column; GE Healthcare, USA) as described above, except that the buffers were supplemented with 1 mM DTT.

Final protein concentrations were determined by measuring the absorbance at 280 nm, using calculated extinction coefficients for the untagged proteins (Pace et al., 1995), which were 11460 M^{-1} cm^{-1} for GB1 Q32C, 27390 M^{-1} cm^{-1} for ERp29 S114C/C157S and ERp29 G147C/C157S, and 67840 M^{-1} cm^{-1} for MBP T237C/T345C and MBP T237U/T345U. The reaction of DCP with two 1,2-aminothiols leads to a conjugated double-bond system (Fig. 1) with a molar extinction coefficient of 6850 M^{-1} cm^{-1} at 280 nm for DCP-(L-Cys)$_2$ and 5400 M^{-1} cm^{-1} for DCP-(L-pen)$_2$, which needs to be considered when determining the concentrations of tagged proteins by UV absorption.

2.2 Synthesis of 4-fluoro-2,6-dicyanopyridine (FDCP), β-cysteine and DCP-(L-Cys)$_2$

FDCP was synthesized from commercially available 4-chloro-2,6-dicyanopyridine (Ambeed, USA) in a single step by heating with CsF as reported elsewhere (Ullrich et al., 2022). The Supporting Information provides protocols for the synthesis of (*S*)-3-amino-4-mercaptobutanoic acid (β-cysteine) and dicyanopyridine ligated with two L-cysteine residues (DCP-(L-Cys)$_2$; Fig. 1).

2.3 FDCP tagging reaction

50 µM solutions of protein were first incubated with 10 mM DTT for 0.5 h to reduce the cysteines, followed by buffer exchange to reaction buffer (50 mM Tris-HCl, pH 7.5, 300 mM NaCl) to remove DTT, using an Amicon ultracentrifugation tube (molecular weight cutoff 3 kDa for GB1 and 10 kDa for all other proteins, using five cycles of five-fold dilution). The tagging reaction was performed with 250 µM FDCP and all ligation reactions were performed at 25 °C, incubating overnight to tag cysteine residues and for 10 minutes to tag selenocysteine residues. Afterwards, excess FDCP was removed by buffer exchange with reaction buffer. In the next step, the DCP-tagged protein was reacted with excess 1,2-aminothiol to obtain the final protein with lanthanide-binding tag. Tags were assembled using five different 1,2-aminothiol compounds, including L-cysteine, D-cysteine, L-penicillamine, D-penicillamine and β-cysteine. The reaction conditions involved 0.5 M 1,2-aminothiol compound, 50 µM DCP-tagged protein, 10 mM TCEP, 50 mM Tris-HCl pH 7.5, 300 mM NaCl and 0.5 h incubation at 25 °C (Fig. 1).

2.4 Mass spectrometry

Whole protein mass spectrometry was performed using an Elite Hybrid Ion Trap-Orbitrap mass spectrometer (Thermo Scientific, USA) coupled with an UltiMate S4 3000 UHPLC (Thermo Scientific, USA). 7.5 pmol of sample were injected to the mass analyser via an Agilent ZORBAX SB-C3 Rapid Resolution HT Threaded Column (Agilent, USA).

Deleted: (

Deleted:

Deleted:

Deleted: and

Formatted: Font: 8 pt

Formatted: Subscript

Deleted: the detailed

Formatted: Font: 8 pt

Formatted: Font: 8 pt

Formatted: Subscript

Deleted: .

2.5 NMR spectroscopy

Deleted: spectrometry

All protein NMR spectra were recorded at 25 °C, using an 800 MHz Bruker Avance NMR spectrometer equipped with a TCI cryoprobe. Samples were prepared in 20 mM HEPES buffer, pH 7.0, in 3 mm NMR tubes. 10 % D_2O was added to provide a lock signal. 0.1–0.5 mM protein samples were used for 2D [^{15}N,^{1}H]-HSQC experiments. 10 mM $LnCl_3$ stock solutions were used to titrate NMR samples.

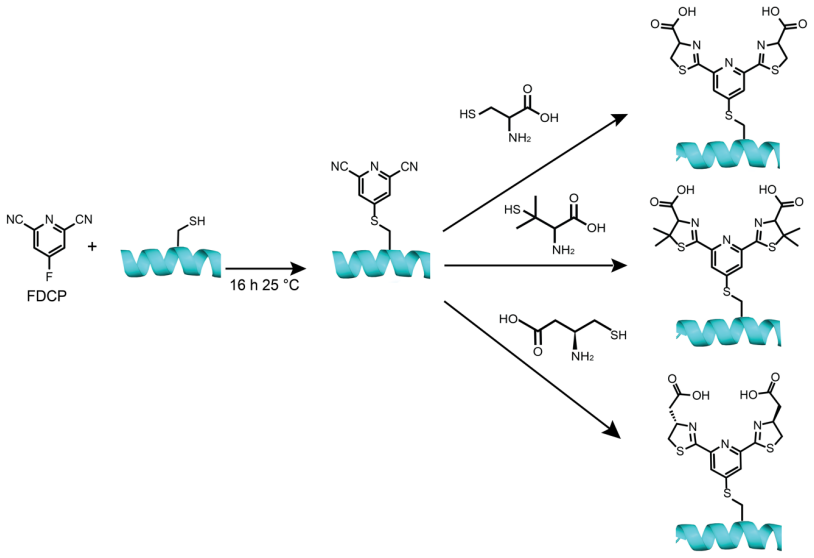

Figure 1. Construction of lanthanide binding motifs on a protein using FDCP. Initially, a solvent-exposed cysteine or selenocysteine residue on the protein is reacted with FDCP. Typical reaction conditions involve incubating the protein at a concentration of 50 µM with 250 µM FDCP at 25 °C and pH 7.5 for 16 h (10 minutes for selenocysteine) to install the DCP tag on the protein. Prior to the tagging reaction, the reduced state of the cysteine thiol group was ensured by treating the protein with 10 mM DTT for 0.5 h followed by extensive buffer exchange to remove DTT. A second step assembles the final lanthanide-binding motif by reacting the FDCP-tagged protein for 0.5 h at 25 °C and pH 7.5 in the presence of 10 mM TCEP with either (top) 0.5 M L- or D-cysteine, (middle) 0.5 M L- or D-penicillamine or (bottom) 0.5 M (*S*)-3-amino-4-mercaptobutanoic acid (β-cysteine).

2.6 PCS measurements and Δχ-tensor fitting

Pseudocontact shifts (PCS) were measured in ppm as the difference in amide proton chemical shift between the paramagnetic and diamagnetic NMR spectrum. PCSs were used to determine the position and orientation of the $\Delta\chi$ tensor of the paramagnetic ions relative to the protein structure. Fitting of $\Delta\chi$ tensors was performed using the program Paramagpy (Orton et al., 2020).

2.7 Residual dipolar coupling measurements

Residual dipolar couplings (RDCs) of one-bond ^{1}H-^{15}N couplings were measured for GB1 Q32C DCP-(L-Cys)$_2$ and GB1 Q32C DCP-(D-pen)$_2$ loaded with Tb^{3+} ions, using the IPAP [^{15}N,^{1}H]-HSQC experiment (Ottiger et al., 1997) with t_{1max} = 75 ms. The RDCs were calculated as the one-bond splittings measured for GB1 with the paramagnetic Tb^{3+} tag minus the corresponding values measured with the diamagnetic Y^{3+} tag. The RDCs were used as input for the program Paramagpy (Orton et al., 2020) to fit alignment tensors and translate them into $\Delta\chi$ tensor parameters (leaving the metal position undetermined).

2.8 DEER measurements

In order to check whether FDCP can be used as a tool for measuring DEER distances, the protein samples were buffer exchanged to 50 mM Tris-HCl in D_2O pD 7.5 (uncorrected pH metre reading) and concentrated to 100 µM following the treatment with excess of L-cysteine or β-cysteine. Gadolinium was added from a 2.5 mM stock solution of $GdCl_3$. Perdeuterated glycerol was added to a final concentration of 20% (v/v) to reach a final protein concentration of 0.1 mM.

All pulsed EPR measurements were carried out at 10 K on a home-built W-band (95 GHz) spectrometer (Goldfarb et al., 2008) equipped with an arbitrary waveform generator (Bahrenberg et al., 2017). Echo-detected EPR (ED-EPR) spectra were recorded using the $\pi/2 - \tau - \pi - \tau -$ echo sequence, with a two-step phase cycle (0,π) on the first π/2 pulse, while keeping τ = 500 ns and sweeping the magnetic field. The durations of the π/2 and π pulses were 15/30 ns, respectively.

DEER measurements employed the standard four-pulse DEER sequence $\pi/2_{vobs} - \tau_1 - \pi_{vobs} - (\tau_1+t) - \pi_{vpump} - (\tau_2-t) - \pi_{vobs} - \tau_2 -$ echo (Pannier et al., 2000). A chirp pump pulse monitoring the echo intensity with increasing delay t and an eight-step phase cycle were applied. The pump pulses with a duration of 128 ns were set to the central transition to cover the range 94.9–95.05 GHz (150 MHz bandwidth) and the observed pulses were set to 94.85 GHz with pulse durations π/2 (π) = 15 (30) ns. The maximum of the Gd^{3+} spectrum was set to 94.9 GHz. The repetition delay was 200 µs and the evolution time depended on the sample. The time domain DEER data were analyzed using the DeerAnalysis2022 software package (Jeschke et al., 2006). The analysis was carried out with the Tikhonov regularization. The background decay was fitted with a dimension of three. Default values were used for the validation process including noise addition. DEER traces were also analyzed with DeerNet (Worswick et al., 2018) through the DeerAnalysis interface.

2.9 Modelling

The experimental DEER distance distributions were compared with distance distributions obtained by crafting models of the Gd^{3+} tags onto crystal structures of the human ERp29 dimer (PDB ID: 2QC7; (Barak et al., 2009)) and MBP (PDB ID: 1OMP; (Sharff et al., 1992)) generating rotamer libraries of the tags with the program PyParaTools as described previously (Stanton-Cook et al., 2014; Welegedara et al., 2021). To predict the Gd^{3+}–Gd^{3+} distances, the tags were crafted onto cysteine residues placed at positions 114 or 147 (for ERp29) and 237 and 345 (for MBP). The rotamer libraries were generated for each tag allowing the χ_1 angle to vary by ±30° around the staggered rotamers, while the χ_2 and χ_3 angles, which precede and follow the sulfur atom respectively (Fig. S13), were allowed to rotate freely. PyParaTools predicts distance distributions by assuming equal population of each tag conformation that is free of van der Waals clashes between tag and protein.

Deleted: S11

3 Results

3.1 Reactivity of FDCP towards cysteine and selenocysteine residues

Cysteine thiol groups react with FDCP in a nucleophilic substitution reaction on the pyridine ring (Fig. 1). To maintain the thiol groups in the reduced state, samples were incubated with DTT and washed with reaction buffer (50 mM Tris-HCl, pH 7.5, 300 mM NaCl) prior to incubation with FDCP. Initially, the reaction conditions were optimized for the mutant GB1 Q32C, where mass spectrometry indicated no reaction product after 10 minutes, incomplete tagging after 6 h and complete reaction following incubation overnight at room temperature (Fig. S3). To test whether selenocysteine is more reactive towards FDCP, calmodulin K148U, where U stands for selenocysteine, was subjected to the same reaction conditions, except that the reaction was conducted in the presence of 1 mM DTT to maintain selenocysteine in the reduced state. The reaction was found to complete within 10 minutes, highlighting the selectivity of FDCP for selenocysteine. There was no evidence of DTT competing with FDCP for ligation with selenocysteine (Fig. S4).

Deleted: S1

Deleted: S2

The role of solvent exposure in the tagging reaction with FDCP was explored using five different proteins containing cysteine residues of varying solvent accessibility. The protein PpiB contains two buried cysteine residues (Cys31 and Cys121). Mass spectrometric analysis indicated that these cysteine residues remain unaffected by the tagging reaction with FDCP (Fig. S5a). The N-terminal domain of *P. falciparum* Hsp90 contains a cysteine residue in position 209, which is near the surface but, according to the crystal structure 3K60 (Corbett et al., 2010), protected from solvent access by a glutamate side chain. The overnight tagging reaction resulted in no tagging (Fig. S5b). The homodimeric rat protein ERp29 contains a single cysteine residue in position 157, which is substantially but not fully solvent exposed. It resulted in about 15 % tagging yield (Fig. S5c). In contrast, ERp29 mutated to contain a cysteine residue in position 114 while the natural cysteine was mutated to serine (mutant S114C/C157S) showed high yield of tagging of Cys114 (Fig. S5d). Residue 114 is very highly solvent-exposed in the NMR structure (1G7E; Liepinsh et al., 2001) and the crystal structure 2QC7 of the human homologue (Barak et al., 2009). The SARS-2 main protease is a cysteine protease containing twelve cysteine residues. Again, FDCP resulted in very little tagging. A small mass spectrometric peak suggested partial tagging of a single cysteine residue (Fig. S5e). In principle, the active-site cysteine is partially solvent-exposed but the crystal structure (6Y2E; Zhang et al., 2020) indicates that three other cysteine

Deleted: S3a

Deleted: S3b

Deleted: S3c

Deleted: S3d

Deleted: S3e

residues are at least as accessible. In contrast, the two highly solvent-exposed cysteine residues of the intracellular domain of $p75^{NTR}$ (Cys379 and Cys416) were both tagged easily (Fig. S5f). These results indicate that complete ligation of FDCP with cysteines can readily be achieved in an overnight reaction, provided that the cysteine thiol groups are highly solvent-exposed.

Deleted: both

Deleted: readily

Deleted: S3f

3.2 Reaction conditions for tag assembly

Following tagging with FDCP, the DCP-tagged proteins were reacted with either cysteine or penicillamine to complete the lanthanoid chelating moiety of the tag (Fig. 1). The necessary reaction conditions were optimised using GB1 Q32C tagged with DCP. 0.5 M cysteine was found to complete the reaction with both cyano groups in half an hour (Fig. S3). To prevent the precipitation of cystine, the reaction buffer was supplemented with 10 mM TCEP, and the pH adjusted to 7.5 if required.

Deleted: S1

High-salt conditions did not accelerate the initial reaction of protein with FDCP, but the following reaction of the cyano groups with cysteine was significantly aided by the presence of salt. For example, none of the cyano groups of the DCP tag reacted in an overnight reaction with 10 mM cysteine and no salt, whereas one of the cyano groups reacted when incubating overnight with 10 mM cysteine in the presence of 300 mM NaCl. Completion of the reaction of both cyano groups in less than one hour required high concentrations of both salt and cysteine (or penicillamine).

3.3 Pseudocontact shifts and RDCs with DCP tags

The potential of the DCP-(L-Cys)$_2$ tag as a lanthanoid tag for the generation of PCSs was investigated using the ^{15}N-labelled GB1 mutant Q32C. Titration of the protein tagged with DCP-(L-Cys)$_2$ with $TbCl_3$ to a metal-to-protein ratio of about 0.6:1 generated PCSs of up to 1.5 ppm in [^{15}N,^{1}H]-HSQC spectra (Table S1, Fig. 2a). At this titration ratio, cross-peaks of the metal-bound protein co-existed with weak cross-peaks of the metal-free protein, indicating slow exchange between proteins with and without metal ion. The experimental PCSs allowed fitting of $\Delta\chi$ tensors with good (i.e., low) quality factors, indicating structural conservation of the protein and little mobility of the tag (Table 1).

Metal-induced aggregation led to protein precipitation at metal-to-protein ratios much greater than 0.6:1. To maintain narrow NMR signals and avoid precipitation, subsequent work focused on samples prepared with metal-to-protein ratios of about 0.6:1.

To explore the potential to vary the chemical and magnetic properties of the tag by changing the 1,2-aminothiol reagent used, we also tested the use of D-cysteine as well as L- and D-penicillamine to complete the DCP tag (Fig. 1). Indeed, the $\Delta\chi$ tensors obtained with DCP-(D-Cys)$_2$ differed in sign, magnitude and orientation from those obtained with DCP-(L-Cys)$_2$ (Table 1 and Fig. 2b), and tag assembly with L- and D-penicillamine again resulted in different $\Delta\chi$ tensors (Table 1 and Fig. 3). As the chemical structure of penicillamine differs from cysteine by two methyl groups in place of the β-hydrogens, penicillamine may be expected to generate a more rigid lanthanide-complexation geometry than cysteine. Some of the $\Delta\chi$ tensors obtained with the tags constructed with penicillamine were quite large, but as the distances between the fitted metal position and the site of tag attachment (Cys32) were also increased, this observation may be attributed to tag flexibility rather

than intrinsically large Δχ tensors. To test this hypothesis, we also measured $^{1}D_{HN}$ RDCs for two of the samples, GB1 Q32C DCP-(L-Cys)$_2$-Tb^{3+} and GB1 Q32C DCP-(D-pen)$_2$-Tb^{3+}. As expected for a poorly determined metal position, the alignment tensors were significantly smaller than predicted from the Δχ tensor determined from PCSs (Table 1). Nonetheless, the Δχ tensor fits of the PCSs of all tags delivered very good *Q* factors despite their mobile character. Furthermore, the z-axes of the tensors obtained with the different tags diverted significantly, with the closest alignment (observed between the DCP-(D-Cys)$_2$ and DCP-(L-pen)$_2$ tags) featuring an angle of 11° between the respective z-axes. The family of tags of the present work thus presents a good basis for generating largely independent Δχ tensors as required for obtaining structural information from multiple tags attached to a single site (Orton et al., 2022).

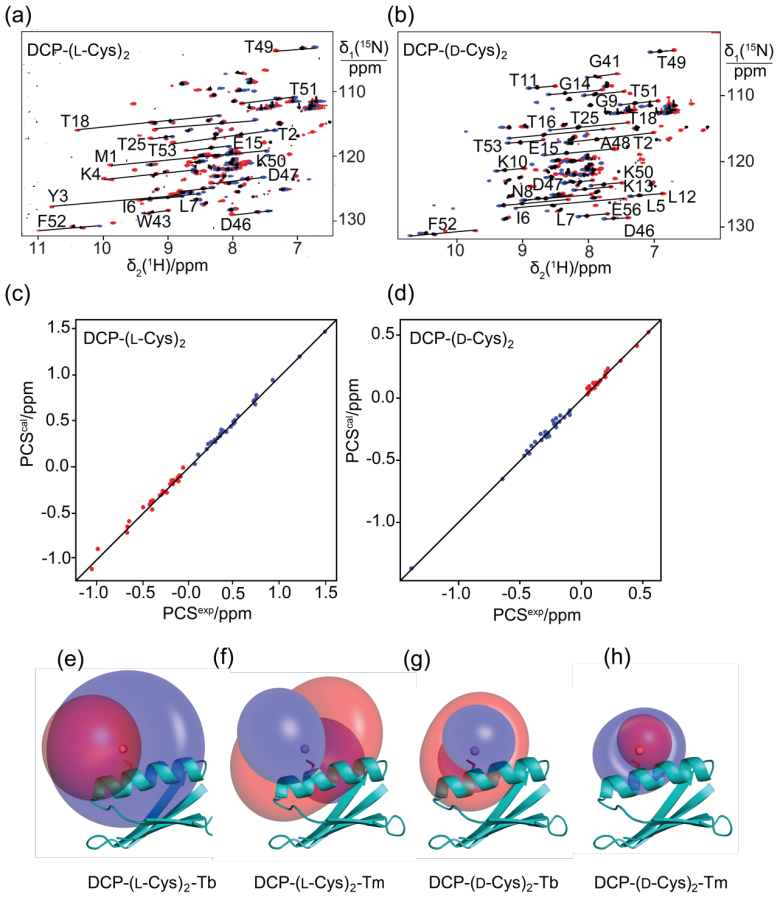

Figure 2. Pseudocontact shifts and Δχ tensors in the protein GB1 Q32C with DCP-Cys tag. (a) Superimposition of [^{15}N,^{1}H]-HSQC spectra of an 0.3 mM solution of GB1 Q32C tagged with DCP-(L-Cys)$_2$ and loaded with either Tb^{3+} (red cross peaks), Tm^{3+} (blue) or Y^{3+} (black). The metal ions were provided in a metal-to-tag ratio of about 0.6:1. Lines connect corresponding cross-peaks observed with diamagnetic and paramagnetic metal ions. (b) Same as (a), but for GB1 Q32C tagged with DCP-(D-Cys)$_2$. (c) Correlation between back-calculated and experimental PCSs of GB1 Q32C tagged with DCP-(L-Cys)$_2$. Red and blue points correspond to the PCSs of Tb^{3+} and Tm^{3+}, respectively. (d) Same as (c), but for the tag assembled with D-

Cys. (e) PCS isosurfaces of ±1 ppm determined by the Δχ tensor of Tb^{3+} bound to the DCP-(L-Cys)$_2$ tag and plotted on a ribbon representation of GB1 Q32C. Positive and negative isosurfaces are shown in blue and red, respectively. The side chain of Cys32 is highlighted with sticks and the metal position obtained by the Δχ tensor fit is identified by a ball. (f) Same as (e), but for Tm^{3+}. (g) Isosurfaces for the tag constructed with D-Cys and loaded with Tb^{3+}. (h) Same as (g), but for Tm^{3+}.

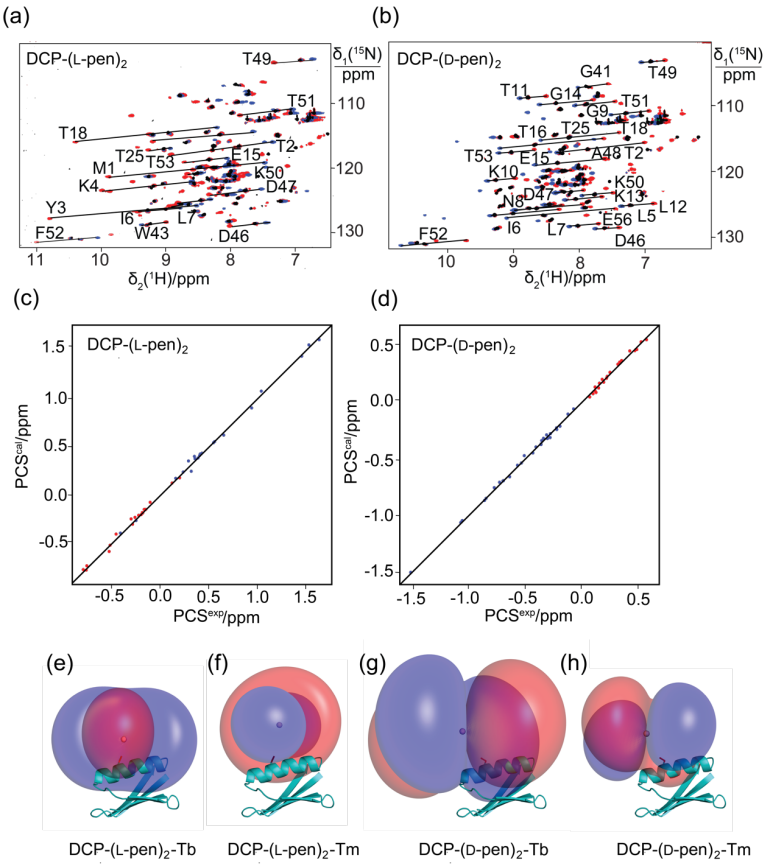

Figure 3. Pseudocontact shifts and Δχ tensors in the protein GB1 Q32C with DCP-penicillamine (DCP-pen$_2$) tag. (a) Superimposition of [^{15}N,^{1}H]-HSQC spectra. Spectra recorded of an 0.3 mM solution of GB1 Q32C tagged with DCP-(L-pen)$_2$ and loaded with either Tb^{3+} (red), Tm^{3+} (blue) or Y^{3+} (black). (b) Same as (a), but for GB1 Q32C tagged with DCP-(D-pen)$_2$.

(c) Correlation between back-calculated and experimental PCSs (Tb^{3+}: red; Tm^{3+}: blue) of GB1 Q32C tagged with DCP-(L-pen)$_2$. (d) Same as (c), but for the tag assembled with D-pen. (e) PCS isosurfaces of +1 ppm (blue) and -1 ppm (red) in GB1 Q32C with DCP-(L-pen)$_2$ tag and Tb^{3+} ion. The side chain of Cys32 is highlighted by a stick representation and a ball marks the metal position obtained from the Δχ-tensor fit. (f) Same as (e), but for Tm^{3+}. (g) Isosurfaces for the tag constructed with D-pen and loaded with Tb^{3+}. (h) Same as (g), but for Tm^{3+}.

Table 1. Δχ-tensor parameters of GB1 Q32C with DCP-Cys$_2$ or DCP-pen$_2$ tags and titrated with Tb^{3+} and Tm^{3+} ions.[1]

Protein construct	$\Delta\chi_{ax}$ (10^{-32} m^3)	$\Delta\chi_{rh}$ (10^{-32} m^3)	x (Å)	y (Å)	z (Å)	α (°)	β (°)	γ (°)	d (Å)	Q
GB1 Q32C DCP-(L-Cys)$_2$-Tb	-21.6	-2.0	35.958	35.881	19.408	34	39	50	10.0	0.05
GB1 Q32C DCP-(L-Cys)$_2$-Tm	16.2	4.7	35.958	35.881	19.408	14	37	37	10.0	0.08
GB1 Q32C DCP-(D-Cys)$_2$-Tb	6.8	1.2	34.322	34.833	19.466	179	114	171	8.1	0.06
GB1 Q32C DCP-(D-Cys)$_2$-Tm	-3.4	-0.5	34.322	34.833	19.466	179	112	141	8.1	0.09
GB1 Q32C DCP-(L-pen)$_2$-Tb	-37.8	-13.6	32.667	39.609	19.491	14	54	68	10.3	0.04
GB1 Q32C DCP-(L-pen)$_2$-Tm	17.7	3.9	32.667	39.609	19.491	10	64	65	10.3	0.08
GB1 Q32C DCP-(D-pen)$_2$-Tb	71.5	37.7	26.888	36.157	7.699	168	69	106	11.9	0.03
GB1 Q32C DCP-(D-pen)$_2$-Tm	-36.4	-20.6	26.888	36.157	7.699	167	70	107	11.9	0.06
GB1 Q32C DCP-(D-pen)$_2$-Tb[2]	15.2	3.9				168	77	28		0.26
GB1 Q32C DCP-(L-Cys)$_2$-Tb[2]	8.1	5.3				0	51	111		0.44

[1] The coordinates of the paramagnetic centre and the Euler angles describing the orientation of the tensor refer to the protein coordinates 1PGA (Gallagher et al., 1994). d is the distance between the β-carbon of residue 32 and the fitted metal position. The fits assumed a common metal position for tags loaded with Tb^{3+} and Tm^{3+} ions. Quality factors Q were calculated as the ratio of the root-mean-square deviation between experimental (Tables S1 and S2) and back-calculated PCSs and the root-mean-square of the experimental PCSs.

[2] Tensor parameters obtained from $^1D_{HN}$ RDC measurements (Table S3). The alignment tensor A was expressed in Δχ tensor units using $\Delta\chi_{ax,rh} = (15\mu_0 k_B T/B_0^2)A_{ax,rh}$, where μ_0 is the induction constant, k_B the Boltzmann constant, T the absolute temperature and B_0 the magnetic field strength (Bertini et al., 2002).

3.4 DCP tags for distance measurements by DEER experiments

The small number of rotatable bonds in the DCP-cysteine and DCP-penicillamine conjugates suggest that the position of the metal ion may be better defined than in tags with longer and less rigid tethers. To test this hypothesis independent of NMR experiments, we prepared samples with two tags, loaded them with Gd^{3+} ions and conducted DEER experiments, where immobile tags can deliver narrow distributions of Gd^{3+}–Gd^{3+} distances, whereas flexible tags invariably result in broad distance

distributions (Welegedara et al., 2017 and 2021; Prokopiou et al., 2018; Widder et al., 2019). The experiments were conducted on a W-band EPR spectrometer following titration of the samples with $GdCl_3$. To start with, we assembled the DCP-(L-Cys)$_2$ tag on the double-mutant G147C/C157S of rat ERp29, which is a homodimer. In addition, we produced the cysteine and selenocysteine mutants of the maltose binding protein, MBP T237C/T345C and MBP T237U/T345U, respectively. Mass spectrometric analysis confirmed complete reaction of all the proteins with FDCP and the subsequent completion of the tags by reaction with 0.5 M cysteine also proceeded in near-quantitative yield (Fig. S6). Samples targeting equimolar ratios of Gd^{3+} ion to tag contained about 20 % excess of Gd^{3+} ions, as the UV absorption of the tag had accidentally been neglected, leading to an overestimation of the protein concentration.

Figure 4 shows the DEER results obtained for ERp29 G147C/C157S, MBP T237U/T345U and MBP T237C/T345C with a 1.2:1 ratio of Gd^{3+} ion to tag and MBP T237C/T345C with a metal-to-tag ratio of 0.6:1. At the 1.2:1 Gd^{3+} ion-to-tag ratio, a narrow distance distribution was observed for ERp29 G147C/C157S, but the distance distribution was broader for MBP T237U/T345U. Unexpectedly, MBP T237C/T345C at the same metal ion-to-tag ratio yielded a distance distribution with two peaks, whereas the same mutant with a sub-stoichiometric ratio of Gd^{3+} ion to tag of 0.6:1 yielded a narrow distance distribution without the additional peak at short distance. The additional peak suggests the existence of an alternative metal binding site that is populated by the excess of Gd^{3+} ions and depleted at lower Gd^{3+} ion concentrations as indicated by the distance distribution observed in Fig. 4d. The narrow distance distribution of Fig. 4d may be aided by dimerization, if DCP-(L-Cys)$_2$ tags of different protein molecules share a single lanthanoid ion as suggested by NMR results obtained with the DCP-(L-Cys)$_2$ ligand (see Section 3.5 below). If this were the case, the positions of the tags could be greatly restricted relative to the protein. Notably, however, the second peak maximum was prominent only in the case of the MBP T237C/T345C mutant, but not in the case of MBP T237U/T345U (Fig. 4b), which is difficult to attribute to differences between selenocysteine and cysteine, although the selenium atom is associated with slightly longer bonds and smaller bond angles.

To guard against coordination of the metal ion by two tag molecules, we reacted the DCP tags with β-cysteine instead of L-cysteine to produce the DCP-(β-Cys)$_2$ tag (Fig. 1c). Figure 5 shows the DEER results obtained with DCP-(β-Cys)$_2$ tags on the mutants ERp29 S114C/C157S and MBP T237C/T345C, following titration of the tags with Gd^{3+} ions. Despite the inaccurate titration ratio, MBP T237C/T345C gave a narrow distance distribution with the maximum at the expected distance (Fig. 5b), with no evidence for a second lanthanoid binding site.

In summary, all samples made with DCP tags featured exceedingly low modulation depths and this was particularly the case for the tags prepared with β-cysteine. In part, this result may be attributed to the relatively broad central transition observed in the ED-EPR spectrum, which is not favourable for DEER experiments. For example, the W-band echo-detected EPR spectra of MBP T237U/T345U and MBP T237C/T345C tagged with DCP-(L-Cys)$_2$-Gd, and ERp29 S114C/C157S labelled with DCP-(β-Cys)$_2$-Gd gave a relative broad central transition with a full width at half-height of 6–7.6 mT (Fig. S8). For comparison, the BrPy-DO3A-Gd and DOTA-maleimide-Gd tags feature central transition linewidths of 4.5 and 1.5 mT, respectively (Giannoulis et al., 2021).

Deleted: S4

Deleted: our

Deleted: S6

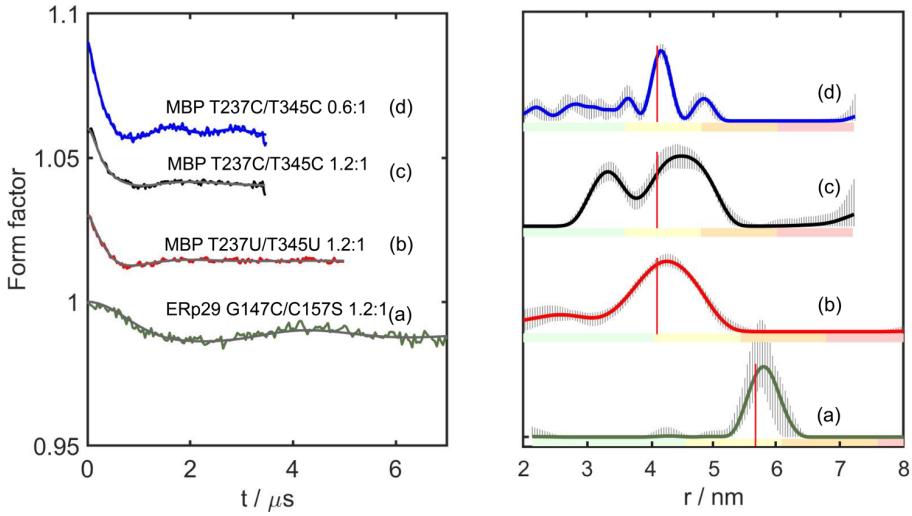

Figure 4. DEER distance measurements with DCP-(L-Cys)$_2$-Gd tags. The left panel shows the form factors after background correction, where the vertical axis plots the normalized echo intensity and the red line corresponds to the fitted trace using the distance distribution calculated by DeerAnalysis2022 (Jeschke et al., 2006) and displayed in the centre panel. The right panel shows the corresponding distance distributions predicted with the program PyParaTools (Fig. S14; Stanton-Cook et al., 2014). The data are annotated with the names of the proteins and the molar ratios of Gd^{3+} ions to DCP-Cys$_2$ tagging sites. (a) ERp29 G147C/C157S with a metal-to-tag ratio of 1.2:1. (b) MBP T237U/T345U with a metal-to-tag ratio of 1.2:1. (c) MBP T237C/T345C with a metal to tag ratio of 1.2:1. (d) Same as (c), but with a metal to tag ratio of 0.6:1. The red vertical lines indicate the maxima of the modelled distance distributions. The colour bar underneath the distance distributions indicates the reliability regions as defined in DeerAnalysis and determined by the DEER evolution time (green: the shape of the distance distribution is reliable; yellow: the mean distance and distribution width are reliable; orange: the mean distance is reliable; red: unreliable long-range distances). The solid lines represent the distributions with the smallest root mean square deviation in relation to the experimental data. The striped regions indicate the range of alternative distributions (±2 times the standard deviation). The primary DEER data are shown in Fig. S9 and the distance analysis by DeerNet (Worswick et al., 2018) is given in Fig. S10.

Deleted: S12

Deleted: S7

Deleted: S8

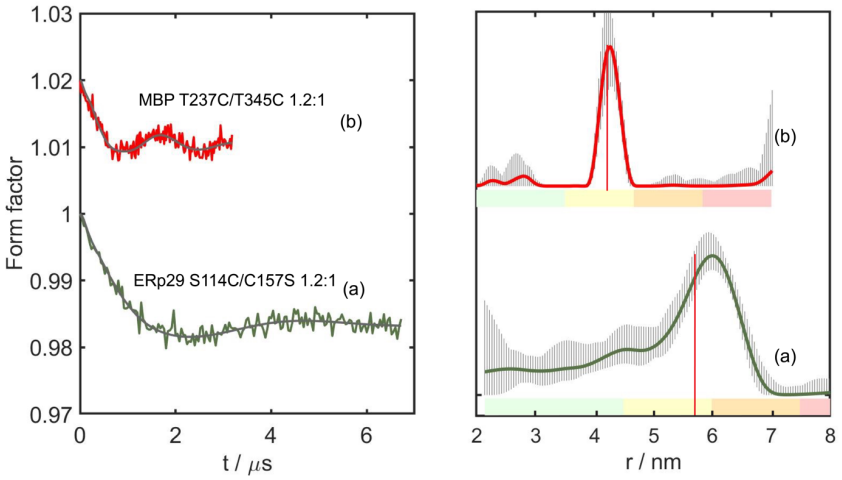

Figure 5. DEER distance measurements with DCP-(β-Cys)$_2$-Gd tags. As in Fig. 4, the left and right panels show the form factors after background subtraction and the distance distribution calculated by DeerAnalysis2018 (Jeschke et al., 2006). All samples were recorded with 1.2:1 Gd^{3+} ion-to-tag ratio. (a) ERp29 S114C/C157S. (b) MBP T237C/T345C. The red vertical lines indicate the maxima of the modelled distance distributions modelled with the program PyParaTools (Fig. S15; Stanton-Cook et al., 2014). The uncertainties in the distance distributions and ranges of alternative distributions are indicated as in Fig. 4. The primary DEER data are shown in Fig. S10 and the distance analysis of (b) by DeerNet (Worswick et al., 2018) in Fig. S12.

Deleted: S13

Deleted: S9

Deleted: S10

3.5 DCP-(L-Cys)$_2$ complex with Y^{3+} ions

To elucidate the stoichiometry of lanthanoid binding by DCP-(L-Cys)$_2$ tags and gain an estimate of the metal binding affinity, we prepared protein-free DCP-(L-Cys)$_2$ and titrated an 0.3 mM solution with YCl_3. Fig. 6 shows that the ^{1}H-NMR spectra of free DCP-(L-Cys)$_2$ are exchange-broadened, which we attribute to 180° flips about the bond between the five-membered rings and the pyridine moiety. A 2-fold excess of Y^{3+} ion freezes this conformation change, and the lines are narrow. The lines labelled D1 and D2 in Fig. 6 belong to a species that we attribute to a 2:1 complex of ligand to metal ion. These signals were less sensitive to attenuation in a diffusion experiment conducted with strong pulsed field gradients (Fig. S16) and greatly decreased when YCl_3 was present in excess (Fig. 6, top spectrum). The residual intensities observed for the free ligand at the titration ratio 0.5:1 indicate that the 2:1 complex is not very stable. An EXCSY spectrum recorded of this sample showed that free and bound ligand exchange with a rate of about 10 s^{-1} (Fig. S17). At the 1:1 titration ratio, any residual intensity of the F1

Formatted: Font: Bold
Formatted: Font: 8 pt, Bold
Formatted: Font: Bold
Formatted: Font: Bold, Subscript
Formatted: Font: Bold
Formatted: Font: Bold, Superscript
Formatted: Font: Bold
Formatted: Font: Not Bold
Formatted: Subscript
Formatted: Superscript
Formatted: Superscript
Formatted: Superscript
Formatted: Subscript
Formatted: Superscript

peak of free DCP-(L-Cys)$_2$ was less than 3 % of the peak integral of the M1 peak. Based on the concentration of ligand and metal used (0.3 mM), the dissociation constant of the 1:1 complex is smaller than 1 μM.

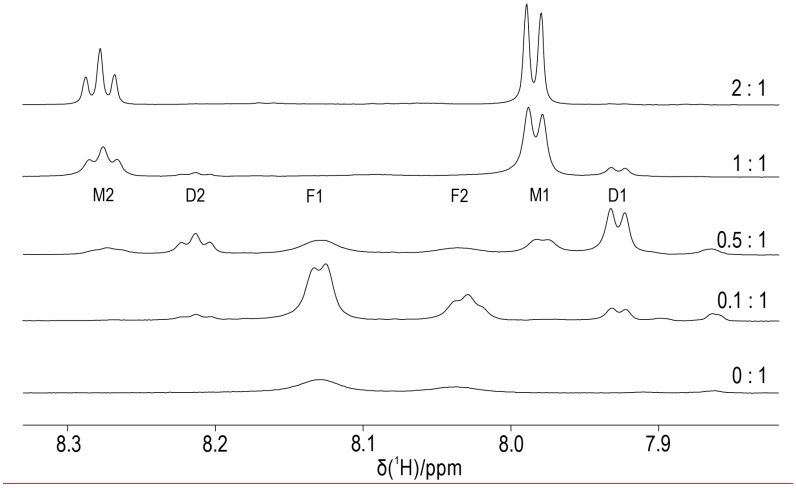

Figure 6. Titration of DCP-(L-Cys)$_2$ with YCl_3. The molar ratios of Y^{3+} ions to DCP tag are indicated on the right. The spectra were recorded of a 0.3 mM sample of DCP-(L-Cys)$_2$ in D_2O containing 10 mM HEPES buffer (pH 7) at 25 °C, using an 800 MHz NMR spectrometer. The spectral region shown contains the signals of the pyridyl ring, which comprise a doublet and a triplet of intensity ratio 2:1. We assign the peaks F1 and F2 to unbound DCP-(L-Cys)$_2$, M1 and M2 to the 1:1 complex with Y^{3+} ion, and D1 and D2 to the complex of two DCP-(L-Cys)$_2$ molecules sharing a single Y^{3+} ion.

4 Discussion

Despite numerous designs of lanthanoid tags and tagging strategies published over the past two decades (Nitsche and Otting, 2017; Su and Chen, 2019; Joss and Häussinger, 2019; Miao et al., 2022) none of the currently available designs simultaneously satisfies all criteria that would make a perfect lanthanoid tag, including rigid attachment to the target molecule via a short tether without causing structural perturbations, chemical selectivity, ease of chemical synthesis and affordability.

The present work assessed a new approach, where the final tag is chemically assembled on the target molecule from different readily accessible building blocks, thus providing easy access to multiple different variants with different paramagnetic properties. Chemical assembly of lanthanide tags on cysteine residues has been proposed previously using pnictogens as mediator between the thiol groups of cysteine and tag, but the pnictogen system depends on a carefully

Formatted: Font: Symbol
Formatted: Centred
Formatted: Font: Bold
Formatted: Font: 8 pt, Bold
Formatted: Font: Bold
Formatted: Font: Bold, Subscript
Formatted: Font: Bold
Formatted: Font: Bold, Subscript
Formatted: Font: Bold
Formatted: Superscript
Formatted: Space After: 0 pt, Line spacing: 1.5 lines
Formatted: Font: 8 pt
Formatted: Subscript
Formatted: Subscript
Formatted: Superscript
Formatted: Superscript

constructed di-cysteine motif, where both cysteine residues need to present their thiol groups in a suitable geometry, as well as assistance by other amino acid side chains of the protein to immobilise the lanthanide ion sufficiently to enable PCS measurements (Nitsche et al., 2017). The approach of the present work is much more straightforward and general, and it enables the construction of a series of different tags that produce different $\Delta\chi$ tensors as required for high-resolution structure analysis of specific sites of interest in a protein (Orton et al., 2022).

FDCP proved to deliver remarkable selectivity for solvent-exposed cysteine residues. For example, FDCP barely reacted with the SARS-2 main protease, which is a cysteine protease where at least four of the twelve cysteine residues are quite solvent-exposed. Similarly, PpiB, which contains two buried cysteine residues, proved completely unreactive towards FDCP, whereas these cysteine residues are known to react readily with maleimide tags under the same conditions (E. H. Abdelkader, personal communication). This observation agrees with the greater spatial demands of a reaction involving a nucleophilic substitution than the addition to an alkene as in, e.g., maleimide tags. In contrast, highly solvent-exposed cysteine thiol groups readily deliver complete reaction yields overnight at room temperature and neutral pH. FDCP thus enables selective targeting of a single highly solvent-exposed cysteine residue without having to mutate numerous native cysteine residues to unreactive amino acids like serine or valine.

Importantly, the reaction of FDCP with selenocysteine was complete within 10 minutes, whereas the reaction with cysteine took more than 6 hours to complete, indicating that selective tagging of selenocysteine can be achieved in the presence of solvent-exposed cysteine residues. A mutant aminoacyl-tRNA synthetase has been shown to install photocaged selenocysteine in proteins in response to an amber stop codon, providing a generally applicable route to genetic encoding of selenocysteine (Welegedara et al., 2018). Only few lanthanoid binding tags are suitable for forming stable ligation products with selenocysteine (Wu et al., 2017; Herath et al., 2021). Work is in progress to increase the protein yields with photocaged selenocysteine, as this would open a most attractive and widely applicable route to site-specific tagging of proteins with a short tether.

While the reactivity of FDCP is high with solvent-exposed cysteine or selenocysteine residues owing to the electron withdrawing effect of the cyano groups, the subsequent reaction of the DCP-labelled protein with cysteine or other 1,2-aminothiols is much slower. We achieved acceptable reaction rates and complete yields by using a generous excess of the β-amino thiol, e.g., 0.5 M cysteine. At concentrations below 100 mM, only one of the cyano groups tended to react with cysteine derivatives. More facile reaction rates have been observed in reactions involving with 1,2-aminothiol compounds without a charged carboxylate group (Morewood et al., 2021; Patil et al., 2021).

The ligation of DCP with two cysteine, penicillamine or β-cysteine molecules creates a binding site for lanthanoid ions. Modelling of the complexes indicates, however, that the nitrogen atoms and carboxyl oxygens cannot be positioned to simultaneously contact the metal ion without breaking the conjugated double-bond system of the pyridine and thiazoline rings (Fig. 1 and S10). The suboptimal coordination geometry may explain why multiple crystallisation attempts of the DCP-(L-Cys)$_2$ complex with Y^{3+} were unsuccessful. The titration of DCP-(L-Cys)$_2$ with YCl_3 indicated the formation of two different complexes, where the Y^{3+} ion is coordinated by either one or two ligand molecules (Fig. 6) with rapid chemical exchange

Deleted: Although t

Formatted: Superscript

between both species. It is tempting to assume that the possibility of two DCP-(L-Cys)$_2$ tags sharing a single lanthanoid ion could contribute to the more uniform and narrower distance distribution obtained for MBP T237C/T345C with DCP-(L-Cys)$_2$-Gd tags for sub-stoichiometric rather than near-equimolar Gd^{3+} ion-to-tag ratios (Fig. 4c and d), but the distance distribution obtained with the selenocysteine version of the construct for the same Gd^{3+} ion-to-tag ratio (Fig. 4b) argues against this interpretation. An alternative explanation could be the difficulty to accurately titrate small sample volumes with $GdCl_3$.

The attempt to break potential dimerization by reacting DCP with β-cysteine instead of cysteine or penicillamine yielded a tag that resulted in loss of NMR signals as soon as paramagnetic lanthanoid ions were added. Therefore, no PCSs could be observed. Using the DCP-(β-Cys)$_2$-Gd tags in DEER experiments indicated that these tags do bind lanthanoid ions and the distance distribution obtained for MBP T237C/T345C was notably narrow and free of multiple maxima for the expected near-equimolar Gd^{3+} ion-to-tag ratio (Fig. 5).

All DEER measurements featured low modulation depths for all DCP-1,2-aminothiol-Gd tags, which can be attributed to the unfavourably broad width of the central transition in the ED-EPR spectrum (Fig. S8) compared with previously established gadolinium tags (Garbuio et al., 2013; Collauto et al., 2016; Shah et al., 2019; Herath et al., 2021), which makes DEER measurements challenging. Furthermore, over-titration or under-titration of the tags with Gd^{3+} ions can also reduce the modulation depths and inaccurate titration ratios arose from ignoring the extinction coefficients of the tags when measuring the protein concentrations by their absorption at 280 nm. In view of the low modulation depths detected in all DEER experiments and the sensitivity of the distance distributions to the actual titration ratio of Gd^{3+} ion to protein, we conclude that these tags are less attractive for DEER distance measurements.

Regarding PCSs, the present work established a new set of tags that are inexpensive, small and relatively rigid, suitable for installation on a highly solvent-exposed cysteine thiol group and capable of delivering Δχ tensor fits with good quality factors. Furthermore, constructing the tags with cysteine or penicillamine generated different PCSs and Δχ tensors of different orientations as required for site-specific structure analysis by PCSs (Orton et al., 2022). The titrations with paramagnetic lanthanoid ions tended to result in broader NMR signals of the paramagnetic species before the complete disappearance of the signals of the free protein. Therefore, the NMR spectra with the narrowest signals were obtained using a substoichiometric lanthanoid-to-tag ratio, which inferred the simultaneous presence of NMR cross-peaks from paramagnetic and diamagnetic species. The greater complexity of the resulting spectra can be addressed by NMR spectra of higher dimensionality in the case of larger proteins (Orton et al., 2018).

Double-arm tags are known to deliver predictable metal positions and Δχ tensor orientations relative to the protein (Keizers et al., 2008), whereas attachment to a single cysteine residue results in unpredictable tag orientations. For the DCP tags of the present work, the limited rigidity of attachment arguably presents an advantage, as it allows generating different Δχ tensor orientations by subtle changes such as completing the tag with 1,2-aminothiols of different chiralities or with different substituents. PCSs obtained with mobile tags are known to deliver excellent structural information so long as an effective Δχ tensor can be fitted that explains the PCSs near the site of interest (Shishmarev and Otting, 2013).

Deleted: was accompanied by significant changes in chemical shifts in the ^{1}H-NMR spectrum and the exchange between the free ligand and the complex was slow on the time scale of chemical shifts, we were unable to determine lanthanoid binding affinities by NMR. In a titration experiment of DCP-(L-Cys)$_2$ with YCl_3, excess of metal ion beyond a ratio of 0.5:1 of metal to DCP-(L-Cys)$_2$ did not lead to further changes of the spectrum, suggesting formation of a stable complex, where a single Y^{3+} ion is coordinated by two DCP-(L-Cys)$_2$ molecules. This not only complicates the analysis but also suggests that a protein with DCP-(L-Cys)$_2$ tag can likewise dimerize by virtue of two DCP-(L-Cys)$_2$ tags sharing a single lanthanoid ion.

Deleted: dimerization

Deleted: remarkably

Deleted: S6

5 Conclusions

The present study shows that significantly different Δχ-tensor orientations can be obtained by transforming the DCP tags with 1,2-aminothiols of different chirality and with different chemical groups. DCP-tag assembly thus establishes a highly attractive concept for producing the multiple different tensor orientations required to determine local protein structure by multiple PCSs (Orton et al., 2022) or analyse protein motions by RDCs (Tolman et al., 2001; Peti et al., 2002; Vögeli et al., 2008). Although FDCP is currently not yet commercially available, its synthesis is straightforward and inexpensive. Finally, the much greater reactivity of FDCP with selenocysteine compared to cysteine suggests that selective tagging of selenocysteine can readily be achieved in the presence of solvent-exposed cysteine residues, which is of great interest for protein studies both by NMR and EPR spectroscopy. The flexibility associated with selective tag assembly encourages the search for further tags constructed by this principle.

Data availability. The NMR and EPR data are available at https://doi.org/10.5281/zenodo.6585976 and https://doi.org/10.5281/zenodo.6579184, respectively.

Supplement. The supplement related to this article is available online at:

Author contributions. SMT prepared the EPR samples, calculated distance distributions and drafted the first version of the manuscript, MCM initiated the project, produced the protein samples for NMR and performed the NMR experiments, resonance assignments and Δχ tensor fits, AF performed the EPR measurements and analysis, AM synthesized β-cysteine, SU synthesized FDCP, RM synthesized DCP-(L-Cys)$_2$, MJM analyzed DCP-(L-Cys)$_2$, TH contributed the concept of different tag assemblies, CN supervised the chemical synthesis at the ANU, DG supervised the EPR data collection, and GO coordinated the project and wrote the final version of the article.

Competing interests. At least one of the (co-)authors is a member of the editorial board of Magnetic Resonance. The authors have no competing interests to declare.

Acknowledgements. We thank Dr. Adarshi Welegedara for the expression vector of calmodulin with amber stop codon and Dr. Angeliki Giannoulis and Ms. Yasmin Ben Ishay for some DEER measurements. Advice by Dr. Josemon George on protocols in organic synthesis is gratefully acknowledged. Gottfried Otting thanks the Australian Research Council, for a Laureate Fellowship (grant no. FL170100019). Ansis Maleckis thanks the European Regional Development Fund for funding. This research was made possible in part by the historic generosity of the Harold Perlman Family (Daniella Goldfarb). Daniella Goldfarb holds the Erich Klieger Professorial Chair in Chemical Physics.

Deleted: for crystallisation
Formatted: Font: 8 pt
Formatted: Subscript

Financial support. This research has been supported by the Australian Research Council (grant no. FL170100019 and DP210100088), the Australian Research Council Centre of Excellence for Innovations in Peptide and Protein Science (grant no. CE200100012) and the European Regional Development Fund (EDRF, PostDoc grant no. 1.1.1.2/VIAA/2/18/381).

References

Abdelkader, E. H., Feintuch, A., Yao, X., Adams, L. A., Aurelio, L., Graham, B., Goldfarb, D., and Otting, G.: Protein conformation by EPR spectroscopy using gadolinium tags clicked to genetically encoded *p*-azido-L-phenylalanine, Chem. Commun., 51, 15898–15901, https://doi.org/10.1039/C5CC07121F, 2015.

Bahrenberg, T., Rosenski, Y., Carmieli, R., Zibzener, K., Qi, M., Frydman, V., Godt, A., Goldfarb, D., and Feintuch, A.: Improved sensitivity for W-band Gd(III)-Gd(III) and nitroxide-nitroxide DEER measurements with shaped pulses, J. Magn. Reson., 283, 1–13, https://doi.org/10.1016/j.jmr.2017.08.003, 2017.

Barak, N. N., Neumann, P., Sevvana, M., Schutkowski, M., Naumann, K., Malešević, M., Reichardt, H., Fischer, G., Stubbs, M. T., and Ferrari, D. M.: Crystal structure and functional analysis of the protein disulfide isomerase-related protein ERp29, J. Mol. Biol., 385, 1630–1642, https://doi.org/10.1016/j.jmb.2008.11.052, 2009.

Bertini, I., Luchinat, C., and Parigi, G.: Magnetic susceptibility in paramagnetic NMR, Prog. Nucl. Magn. Reson. Spectrosc., 40, 211–236, https://doi.org/10.1016/S0079-6565(02)00002-X, 2002.

Collauto, A., Frydman, V., Lee, M., Abdelkader, E., Feintuch, A., Swarbrick, J., Graham, B., Otting, G., and Goldfarb, D.: RIDME distance measurements using Gd(III) tags with a narrow central transition, Phys. Chem. Chem. Phys., 18, 19037–19049, https://doi.org/10.1039/C6CP03299K, 2016.

Corbett, K. D. and Berger, J. M.: Structure of the ATP-binding domain of *Plasmodium falciparum* Hsp90, Proteins, 78, 2738–2744, https://doi.org/10.1002/prot.22799, 2010.

Feintuch, A., Otting, G., and Goldfarb, D.: Gd^{3+} spin labeling for measuring distances in biomacromolecules: why and how?, Methods Enzymol., 415–457, https://doi.org/10.1016/bs.mie.2015.07.006, 2015.

Gallagher, T., Alexander, P., Bryan, P., and Gilliland, G. L.: Two crystal structures of the B1 immunoglobulin-binding domain of streptococcal protein G and comparison with NMR, Biochemistry, 33, 4721–4729, https://doi.org/10.1021/bi00181a032, 1994.

Garbuio, L., Bordignon, E., Brooks, E. K., Hubbell, W. L., Jeschke, G., and Yulikov, M.: Orthogonal spin labeling and Gd(III)–nitroxide distance measurements on bacteriophage T4-lysozyme, J. Phys. Chem. B, 117, 3145–3153, https://doi.org/10.1021/jp401806g, 2013.

Giannoulis, A., Ben-Ishay, Y., and Goldfarb, D.: Characteristics of Gd(III) spin labels for the study of protein conformations, Methods Enzymol., 651, 235–290, https://doi.org/10.1016/bs.mie.2021.01.040, 2021.

Goldfarb, D., Lipkin, Y., Potapov, A., Gorodetsky, Y., Epel, B., Raitsimring, A. M., Radoul, M., and Kaminker, I.: HYSCORE and DEER with an upgraded 95 GHz pulse EPR spectrometer, J. Magn. Reson., 194, 8–15, https://doi.org/10.1016/j.jmr.2008.05.019, 2008.

Guignard, L., Ozawa, K., Pursglove, S. E., Otting, G., and Dixon N. E.: NMR analysis of *in vitro*-synthesized proteins without purification: a high-throughput approach, FEBS Lett., 524, 159–162, https://doi.org/10.1016/S0014-5793(02)03048-X, 2002.

Herath, I. D., Breen, C., Hewitt, S. H., Berki, T. R., Kassir, A. F., Dodson, C., Judd, M., Jabar, S., Cox, N., and Otting, G.: A chiral lanthanide tag for stable and rigid attachment to single cysteine residues in proteins for NMR, EPR and time-resolved luminescence studies, Chem. Eur. J., 27, 13009–13023, https://doi.org/10.1002/chem.202101143, 2021.

Jeschke, G., Chechik, V., Ionita, P., Godt, A., Zimmermann, H., Banham, J., Timmel, C., Hilger, D., and Jung, H.: DeerAnalysis2006 – a comprehensive software package for analyzing pulsed ELDOR data, Appl. Magn. Reson., 30, 473–498, https://doi.org/10.1007/BF03166213, 2006.

Johansen-Leete, J., Ullrich, S., Fry, S. E., Frkic, R., Bedding, M. J., Aggarwal, A., Ashhurst, A. S., Ekanyake, K. B., Mahawaththa, M. C., Sasi, V. M., Passioura, T., Larance, M., Otting, G., Turville, S., Jackson, C. J., Nitsche, C., and Payne R. J.: Antiviral cyclic peptides targeting the main protease of SARS-CoV-2, Chem. Sci., 13, 3826–3836, https://doi.org/10.1039/DISC06750H, 2022.

Jones, D. H., Cellitti, S. E., Hao, X., Zhang, Q., Jahnz, M., Summerer, D., Schultz, P. G., Uno, T., and Geierstanger, B. H.: Site-specific labeling of proteins with NMR-active unnatural amino acids, J. Biomol. NMR, 46, 89–100, https://doi.org/10.1007/s10858-009-9365-4, 2010.

Joss, D. and Häussinger, D.: Design and applications of lanthanide chelating tags for pseudocontact shift NMR spectroscopy with biomacromolecules, Prog. Nucl. Mag. Res. Sp., 114–115, 284–312, https://doi.org/10.1016/j.pnmrs.2019.08.002, 2019.

Keizers, P. H. J., Saragliadis, A., Hiruma, Y., Overhand, M., and Ubbink, M.: Design, synthesis, and evaluation of a lanthanide chelating protein probe: CLaNP-5 yields predictable paramagnetic effects independent of environment, J. Am. Chem. Soc., 130, 14802–14812, https://doi.org/10.1021/ja8054832, 2008.

Klopp, J., Winterhalter, A., Gébleux, R., Scherer-Becker, D., Ostermeier, C., and Gossert, A. D.: Cost-effective large-scale expression of proteins for NMR studies, J. Biomol. NMR, 71, 247–262, https://doi.org/10.1007/s10858-018-0179-0, 2018.

Liepinsh, E., Baryshev, M., Sharipo, A., Ingelman-Sundberg, M., Otting, G., and Mkrtchian S.: Thioredoxin-fold as a homodimerization module in the putative chaperone ERp29: NMR structures of the domains and experimental model of the 51 kDa homodimer, Structure, 9, 457–471, https://doi.org/10.1016/S0969-2126(01)00607-4, 2001.

Mekkattu Tharayil, S., Mahawaththa, M. C., Loh, C. T., Adekoya, I., and Otting, G.: Phosphoserine for the generation of lanthanide-binding sites on proteins for paramagnetic nuclear magnetic resonance spectroscopy, Magn. Reson., 2, 1–13, https://doi.org/10.5194/mr-2-1-2021, 2021.

Miao, Q., Nitsche, C., Orton, H., Overhand, M., Otting, G., and Ubbink, M.: Paramagnetic chemical probes for studying biological macromolecules, Chem. Rev., in press, https://doi.org/10.1021/acs.chemrev.1c00708, 2022.

Morewood, R. and Nitsche, C.: A biocompatible stapling reaction for *in situ* generation of constrained peptides, Chem. Sci., 12, 669–674, https://doi.org/10.1039/D0SC05125J, 2021.

Neylon, C., Brown, S. E., Kralicek, A. V., Miles, C. S., Love, C. A., and Dixon, N. E.: Interaction of the *Escherichia coli* replication terminator protein (Tus) with DNA: a model derived from DNA-binding studies of mutant proteins by surface plasmon resonance, Biochemistry, 39, 11989–11999, https://doi.org/10.1021/bi001174w, 2000.

Nitsche, C., Mahawaththa, M. C., Becker, W., Huber, T., and Otting, G.: Site-selective tagging of proteins by pnictogen-mediated self-assembly, Chem. Commun., 53, 10894–10897, https://doi.org/10.1039/C7CC06155B, 2017.

Nitsche, C. and Otting, G.: Pseudocontact shifts in biomolecular NMR using paramagnetic metal tags, Prog. Nucl. Mag. Res. Sp., 98–99, 20–49, https://doi.org/10.1016/j.pnmrs.2016.11.001, 2017.

Nitsche, C., Onagi, H., Quek, J.-P., Otting, G., Dahai, L., and Huber, T.: Biocompatible macrocyclization between cysteine and 2-cyanopyridine generates stable peptide inhibitors, Org. Lett., 21, 4709–4712, https://doi.org/10.1021/acs.orglett.9b01545, 2019.

Orton, H. W. and Otting, G.: Accurate electron–nucleus distances from paramagnetic relaxation enhancements, J. Am. Chem. Soc, 140, 7688–7697, https://doi.org/10.1021/jacs.8b03858, 2018.

Orton, H. W., Huber, T., and Otting, G.: Paramagpy: software for fitting magnetic susceptibility tensors using paramagnetic effects measured in NMR spectra, Magn. Reson., 1, 1–12, https://doi.org/10.5194/mr-1-1-2020, 2020.

Orton, H. W., Abdelkader, E. H., Topping, L., Butler, S. J., and Otting, G.: Localising nuclear spins by pseudocontact shifts from a single tagging site, Magn. Reson., 3, 65–76, https://doi.org/10.5194/mr-3-65-2022, 2022.

Ottiger, M., Delaglio, F., and Bax, A.: Measurement of *J* and dipolar couplings from simplified two-dimensional NMR spectra, J. Magn. Reson., 131, 373–378, https://doi.org/10.1006/jmre.1998.1361, 1998.

Otting, G.: Protein NMR using paramagnetic ions, Annu. Rev. Biophys. Biol. Struct., 39, 387–405, https://doi.org/10.1146/annurev.biophys.093008.131321, 2010.

Pace, C.N., Vajdos, F., Fee, L., Grimsley, G., and Gray, T.: How to measure and predict the molar absorption coefficient of a protein, Protein Sci. 11, 2411-2423, https://doi.org/10.1002/pro.5560041120, 1995.

Pannier, M., Veit, S., Godt, A., Jeschke, G., and Spiess, H. W.: Dead-time free measurement of dipole-dipole interactions between electron spins, J. Magn. Reson., 142, 331–340, https://doi.org/10.1006/jmre.1999.1944, 2000.s

Patil, N. A., Quek, J.P., Schroeder, B., Morewood, R., Rademann, J., Luo, D., and Nitsche, C.: 2-Cyanoisonicotinamide conjugation: a facile approach to generate potent peptide inhibitors of the Zika virus protease, ACS Med. Chem. Lett., 12, 732–737, https://doi.org/10.1021/acsmedchemlett.0c00657, 2021.

Peti, W., Meiler, J., Brüschweiler, R., and Griesinger, C.: Model-free analysis of protein backbone motion from residual dipolar couplings, J. Am. Chem. Soc., 124, 5822–5833, https://doi.org/10.1021/ja011883c, 2002.

Potapov, A., Yagi, H., Huber, T., Jergic, S., Dixon, N. E., Otting, G., and Goldfarb, D.: Nanometer scale distance measurements in proteins using Gd^{3+} spin labelling, J. Am. Chem. Soc., 132, 9040–9048, https://doi.org/10.1021/ja1015662, 2010.

Prokopiou, G., Lee, M. D., Collauto, A., Abdelkader, E. H., Bahrenberg, T., Feintuch, A., Ramirez-Cohen, M., Clayton, J., Swarbrick, J. D., and Graham, B.: Small Gd(III) tags for Gd(III)–Gd(III) distance measurements in proteins by EPR spectroscopy, Inorg. Chem., 57, 5048–5059, https://doi.org/10.1021/acs.inorgchem.8b00133, 2018.

Qi, R. and Otting, G.: Mutant T4 DNA polymerase for easy cloning and mutagenesis, PLOS One, 14, e0211065, https://doi.org/10.1371/journal.pone.0211065, 2019.

Shah, A., Roux, A., Starck, M., Mosely, J. A., Stevens, M., Norman, D. G., Hunter, R. I., El Mkami, H., Smith, G. M., and Parker, D.: A gadolinium spin label with both a narrow central transition and short tether for use in double electron electron resonance distance measurements, Inorg. Chem., 58, 3015–3025, https://doi.org/10.1021/acs.inorgchem.8b02892, 2019.

Sharff, A. J., Rodseth, L. E., Spurlino, J. C., and Quiocho, F. A.: Crystallographic evidence of a large ligand-induced hinge-twist motion between the two domains of the maltodextrin binding protein involved in active transport and chemotaxis, Biochemistry, 31, 10657–10663, https://doi.org/10.1021/bi00159a003, 1992.

Shishmarev, D. and Otting, G.: How reliable are pseudocontact shifts induced in proteins and ligands by mobile paramagnetic tags? A modelling study, J. Biomol. NMR, 56, 203–216, https://doi.org/10.1007/s10858-013-9738-6, 2013.

Stanton-Cook, M. J., Su, X.-C., Otting, G., and Huber, T.: PyParaTools, available at http://comp-bio.anu.edu.au/mscook/PPT/ (last access: 1 May 2022), 2014.

Su, X.-C. and Chen, J.-L.: Site-specific tagging of proteins with paramagnetic ions for determination of protein structures in solution and in cells, Acc. Chem. Res., 52, 1675–1686, https://doi.org/10.1021/acs.accounts.9b00132, 2019.

Tolman, J. R., Al-Hashimi, H. M., Kay, L. E., and Prestegard, J. H.: Structural and dynamic analysis of residual dipolar coupling data for proteins, J. Am. Chem. Soc., 123, 1416–1424, https://doi.org/10.1021/ja002500y, 2001.

Ullrich, S., George, J., Coram, A., Morewood, R., and Nitsche, C.: Biocompatible and selective generation of bicyclic peptides, Angew. Chem. Int. Ed., https://doi.org/10.1002/ange.202208400, 2022.

Vögeli, B., Yao, L., and Bax, A.: Protein backbone motions viewed by intraresidue and sequential HN-Ha residual dipolar couplings, J. Biomol. NMR, 41, 17–28, https://doi.org/10.1007/s10858-008-9237-3, 2008.

Welegedara, A. P., Adams, L. A., Huber, T., Graham, B., and Otting, G.: Site-specific incorporation of selenocysteine by genetic encoding as a photocaged unnatural amino acid, Bioconjugate Chem., 29, 2257–2264, https://doi.org/10.1021/acs.bioconjchem.8b00254, 2018.

Welegedara, A. P., Yang, Y., Lee, M. D., Swarbrick, J. D., Huber, T., Graham, B., Goldfarb, D., and Otting, G.: Double-arm lanthanide tags deliver narrow Gd^{3+}–Gd^{3+} distance distributions in double electron–electron resonance (DEER) measurements, Chem. Eur. J., 23, 11694–11702, https://doi.org/10.1039/c5cp02602d, 2017.

Welegedara, A. P., Maleckis, A., Bandara, R., Mahawaththa, M. C., Herath, I. D., Jiun Tan, Y., Giannoulis, A., Goldfarb, D., Otting, G., and Huber, T.: Cell-Free synthesis of selenoproteins in high yield and purity for selective protein tagging, ChemBioChem, 22, 1480–1486, https://doi.org/10.1002/cbic.202000785, 2021.

Deleted: ChemRxiv

Deleted: 26434/chemrxiv-2022-xw6cm

Widder, P., Berner, F., Summerer, D., and Drescher, M.: Double nitroxide labeling by copper-catalyzed azide–alkyne cycloadditions with noncanonical amino acids for electron paramagnetic resonance spectroscopy, ACS Chem. Biol., 14, 839–844, https://doi.org/10.1021/acschembio.8b01111, 2019.

Worswick, S. G., Spencer, J. A., Jeschke, G., and Kuprov, I.: Deep neural network processing of DEER data, Sci. Adv., 4, eaat5218, https://doi.org/10.1126/sciadv.aat5218, 2018.

Wu, Z., Lee, M. D., Carruthers, T. J., Szabo, M., Dennis, M. L., Swarbrick, J. D., Graham, B., and Otting, G.: New lanthanide tag for the generation of pseudocontact shifts in DNA by site-specific ligation to a phosphorothioate group, Bioconjugate Chem., 28, 1741–1748, https://doi.org/10.1021/acs.bioconjchem.7b00202, 2017.

Yagi, H., Banerjee, D., Graham, B., Huber, T., Goldfarb, D., and Otting, G.: Gadolinium tagging for high-precision measurements of 6 nm distances in protein assemblies by EPR, J. Am. Chem. Soc., 133, 10418–10421, https://doi.org/10.1021/ja204415w, 2011.

Zhang, L., Lin, D., Sun, X., Curth, U., Drosten, C., Sauerhering, L., Becker, S., Rox, K., and Hilgenfeld, R.: Crystal structure of SARS-CoV-2 main protease provides a basis for design of improved α-ketoamide inhibitors, Science, 368, 409–412, https://doi.org/10.1126/science.abb3405, 2020.

Supporting Information

Table of contents

Formatted: Font: Italic
Formatted: Font: Symbol
Formatted: Font: Bold
Formatted: Font: 10 pt, Bold
Formatted: Font: Bold
Formatted: Font: Bold, Subscript
Formatted: Font: Bold
Formatted: Font: Not Bold
Deleted: S1
Deleted: S2
Deleted: S3
Deleted: S4
Deleted: S5
Deleted: S6
Deleted: S7
Deleted: S8
Deleted: S9
Deleted: S10

Deleted: S11

Deleted: S12

Deleted: S13

Formatted: Font: Not Bold

Formatted: Font: Bold

Formatted: Subscript

Formatted: Subscript

Formatted: Font: Bold

Synthesis of (*S*)-3-amino-4-mercaptobutanoic acid hydrochloride (β-cysteine, 5)

A synthesis of β-cysteine was described by Birkofer and Birkofer (1956) without spectroscopic characterisation data of the final compound. Below is a detailed description of the synthetic route chosen in the present work.

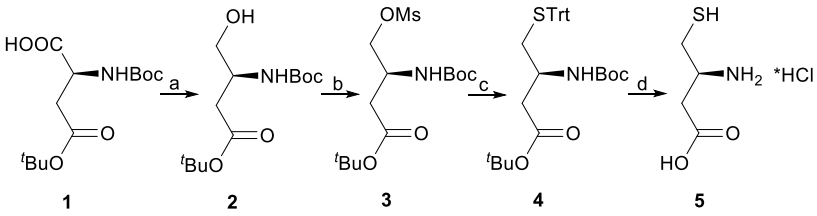

Reagents and conditions: **a)** *N*-methyl morpholine (1.3 equiv), ethyl chloroformate (1.2 equiv), THF, 0 °C, 30 min. then $NaBH_4$ (2 equiv) in water, 0 °C, 30 min, 73 %; **b)** DIPEA (1.7 equiv), methanesulfonyl chloride (1.2 equiv), toluene, 0 °C, 2 h, 85 %; **c)** triphenylmethanethiol (1.8 equiv), KO^{t}Bu (1.6 equiv), THF, 0 °C, 30 min., 71 %; **d)** triethylsilane/TFA, DCM, 5 h, then anhydrous HCl/Et_2O, 71 %.

***tert*-Butyl (*S*)-3-((*tert*-butoxycarbonyl)amino)-4-hydroxybutanoate (2)**

Ethyl chloroformate (1.90 mL; 20 mmol) was added dropwise to a cooled (0 °C) solution of Boc-*L*-aspartic acid 4-*tert*-butyl ester (**1**) (5.00 g; 17.3 mmol) and *N*-methyl morpholine (2.40 mL; 22.0 mmol) in THF (150 mL). The resulting mixture was stirred at 0 °C for 30 minutes when it was pured into a cooled solution of $NaBH_4$ (1.32 g; 35.0 mmol) in water (50 mL) with intensive stirring. The resulting emulsion was stirred intensively for 30 minutes and THF was subsequently removed under reduced pressure. The residue was partitioned between brine (100 mL) and EtOAc (200 mL). The organic phase was washed with aq $KHSO_4$ (5 %; 2 x 100 mL), saturated aq $NaHCO_3$ (100 mL) and brine (100 mL) and evaporated under reduced pressure. The crude product was purified by flash column chromatography (mobile phase hexanes/EtOAc with gradient from 4/1 to 1/1). 3.46 g (73 %) of colourless amorphous solid was obtained. For ^{1}H-NMR data, see Bergeron et al. (1998).

***tert*-Butyl (*S*)-3-((*tert*-butoxycarbonyl)amino)-4-((methylsulfonyl)oxy)butanoate (3)**

Methanesulfonyl chloride (1.1 mL; 14 mmol) was added dropwise to a cooled (0 °C) solution of *tert*-butyl (*S*)-3-((*tert*-butoxycarbonyl)amino)-4-hydroxybutanoate (**2**) (3.25 g; 11.8 mmol) and DIPEA (3.5 mL; 20 mmol) in toluene (150 mL). The reaction was stirred at 0 °C for 2

Formatted: Font: Not Bold
Formatted: Font: Symbol, Not Bold
Formatted: Font: Not Bold
Formatted: Justified
Formatted: Font: Not Bold
Formatted: Superscript

hours. TLC analysis showed complete conversion. The reaction mixture was partitioned between aq $KHSO_4$ (5 %; 150 mL) and EtOAc (150 mL). The organic phase was washed with aq $KHSO_4$ (5 %; 100 mL), saturated aq $NaHCO_3$ (100 mL) and brine (100 mL) and evaporated under reduced pressure. The residue was purified by flash column chromatography (mobile phase hexanes/EtOAc with gradient from 4/1 to 1/1). 3.56 g (85 %) of yellowish oil was obtained. For ^{1}H-NMR data, see Kim et al. (2014).

Formatted: Superscript

***tert*-Butyl (*S*)-3-((*tert*-butoxycarbonyl)amino)-4-(tritylthio)butanoate (4)**

Potassium *tert*-butoxide (1.7g; 15 mmol) was added portionwise to a cooled (-20 °C) solution of triphenylmethanethiol (4.7 g; 17 mmol) in dry THF (150 mL). The reaction mixture was stirred until all solids dissolved and subsequently slowly cannulated into a cooled solution (0 °C) of *tert*-butyl (*S*)-3-((*tert*-butoxycarbonyl)amino)-4-((methylsulfonyl)oxy)butanoate (**3**) (3.40 g; 9.62 mmol) in dry THF (50 mL). The resulting solution was stirred at 0 °C for about 30 minutes. At this point TLC analysis indicated complete conversion of **3**. The reaction mixture was quenched by the addition of saturated aq $NaHCO_3$ (100 mL) and THF was removed under reduced pressure. The residue was partitioned between brine (100 mL) and EtOAc (200 mL). The organic phase was washed with saturated aq $NaHCO_3$ (100 mL) and brine (100 mL) and evaporated under reduced pressure. The crude product was purified by flash column chromatography (mobile phase hexanes/EtOAc with gradient from 20/1 to 4/1). 3.62 g (71 %) of white foam was obtained.

(*S*)-3-Amino-4-mercaptobutanoic acid hydrochloride (5)

Trifluoroacetic acid (8 mL) was added to a cooled (0 °C) solution of *tert*-butyl (*S*)-3-((*tert*-butoxycarbonyl)amino)-4-(tritylthio)butanoate (**4**) (3.60 g; 6.75 mmol) and triethylsilane (5 mL) in DCM (30 mL). The reaction mixture was stirred at ambient temperature 5 h. LC-MS analysis indicated complete conversion. The volatiles were removed under reduced pressure. The residue was dissolved in EtOAc (50 mL) and anhydrous HCl (2 M in ether; 6 mL) was added. The volatiles were removed under reduced pressure and the HCl treatment was repeated 3 times. The glue-like residue was suspended in EtOAc (30 mL) and sonicated 30 minutes which promoted crystallization of the amorphous substance. The reaction product was collected by centrifugation and it was washed with additional EtOAc (2 x 5 mL). After drying under vacuum 1.05 g (91 %) of white microcrystalline solid was obtained.

Deleted: ¶
¶
Page Break

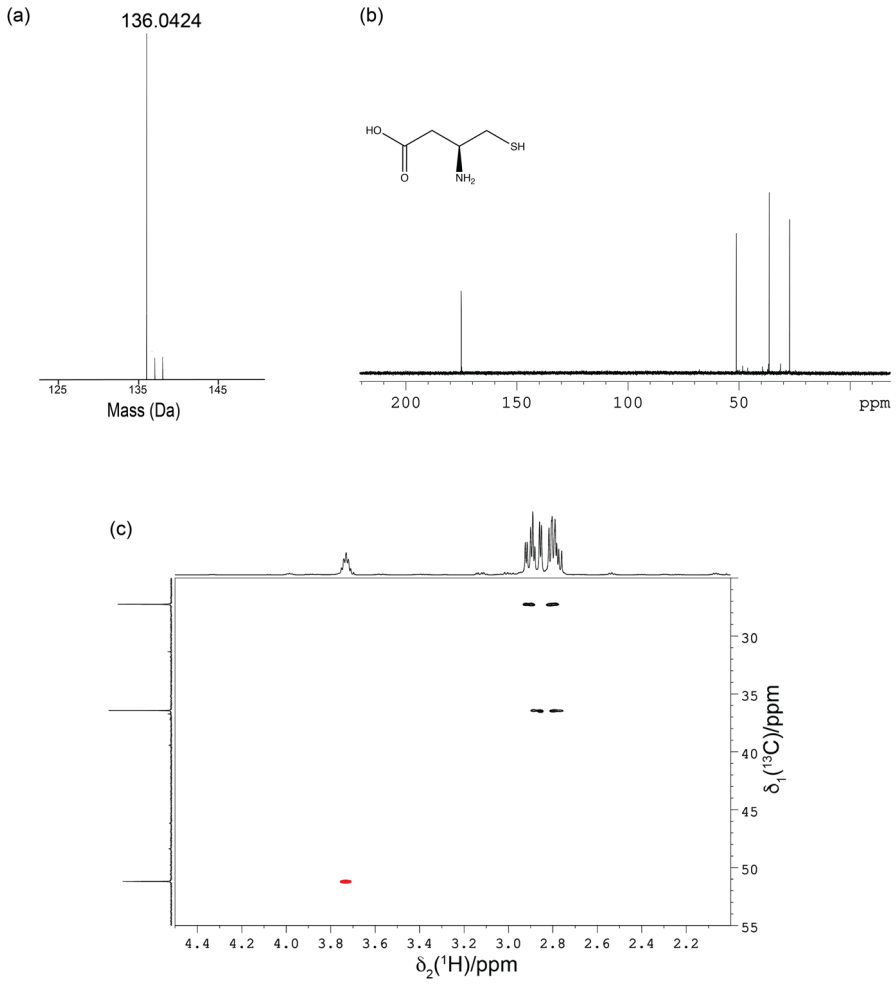

Figure S1. Mass spectrometric and NMR analysis of (*S*)-3-amino-4-mercaptobutanoic acid (β-cysteine). (a) HR-ESI mass spectrum of β-cysteine. The calculated mass is 135.18 Da. (b) and (c) show, respectively, the 1D ^{13}C-NMR spectrum and [^{13}C,^{1}H]-HSQC spectrum recorded of a 5 mM sample of β-cysteine prepared in D_2O.

Synthesis of DCP-(L-Cys)$_2$

2,6-pyridinedicarbonitrile (41.0 mg, 0.317 mmol) and L-cysteine hydrochloride (100 mg, 0.634 mmol) were added to 2 ml MeOH/water (1:1). The pH was adjusted to 7 with KOH and the mixture was stirred for 3 days. The solvent was removed under reduced pressure and the crude product was purified using a 10 g silica gel cartridge (5–20 % water:EtOH) to yield the title compound (44.2 mg, 41 %) as an off-white crystalline powder.

LRMS (ESI) *m/z*: 338.0 $[M+H]^+$

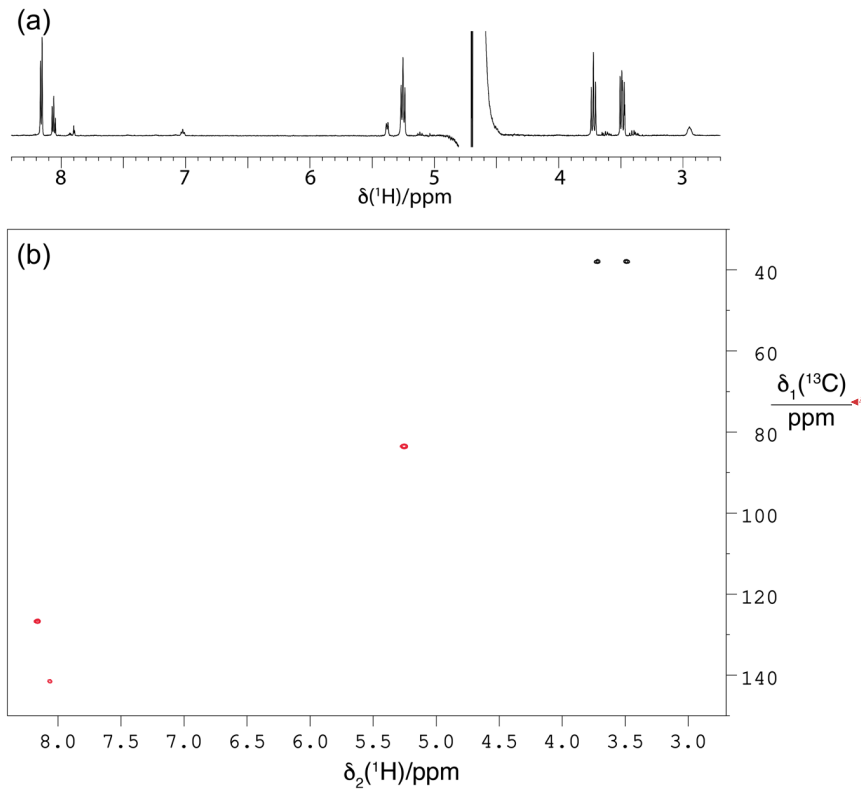

Figure S2. NMR spectra of 0.6 mM DCP-(L-Cys)$_2$ in D_2O at 25 ºC. Spectra recorded on a 600 MHz NMR spectrometer. (a) ^{1}H-NMR spectrum with presaturation of the HDO signal. Small signals at about 7, 5.4 and 2.9 ppm are from a minor conformer that is in chemical exchange with the main species. (b) [^{13}C,^{1}H]-HSQC spectrum. Positive (black) and negative (red) cross-peaks are from CH_2 and CH groups, respectively.

Formatted: Font: Bold
Formatted: Line spacing: 1.5 lines
Formatted: Font: (Default) Times New Roman, 12 pt
Formatted: Font: (Default) Times New Roman, 10 pt
Formatted: Font: (Default) Times New Roman, 12 pt
Formatted: Justified, Line spacing: 1.5 lines
Formatted: Font: (Default) Times New Roman, 12 pt
Formatted: Font: (Default) Times New Roman, 12 pt
Formatted: Font: (Default) Times New Roman, 12 pt
Formatted: Font: (Default) Times New Roman, 12 pt
Formatted: Font: (Default) Times New Roman, 12 pt
Formatted: Font: (Default) Times New Roman, 12 pt
Formatted: Font: (Default) Times New Roman, 12 pt
Formatted: Line spacing: 1.5 lines
Formatted: Left
Formatted: Font: Not Bold
Formatted: Font: Not Bold
Formatted: Font: Not Bold
Formatted: Subscript
Formatted: Superscript
Formatted: Superscript
Formatted: Superscript
Formatted: Superscript
Formatted: Subscript

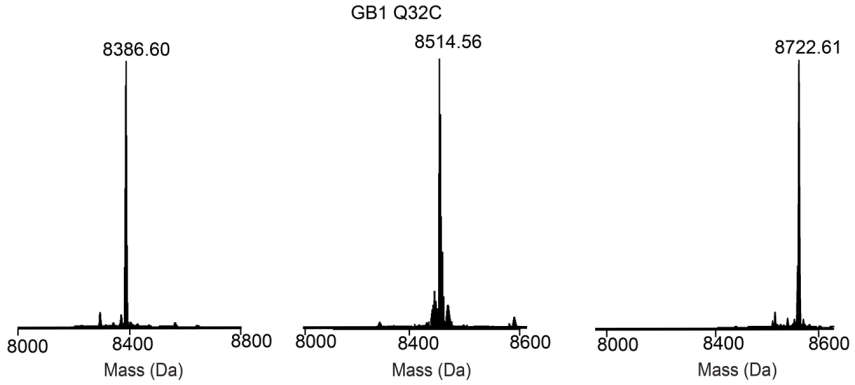

Figure S3. Deconvoluted intact protein mass spectra of uniformly ^{15}N-labelled GB1 Q32C. Left panel: before tagging reaction with FDCP. Centre panel: after reaction with FDCP. Right panel: after the complete assembly of the DCP-(L-Cys)$_2$ tag on the protein (expected mass increase 336 Da).

Deleted: S1

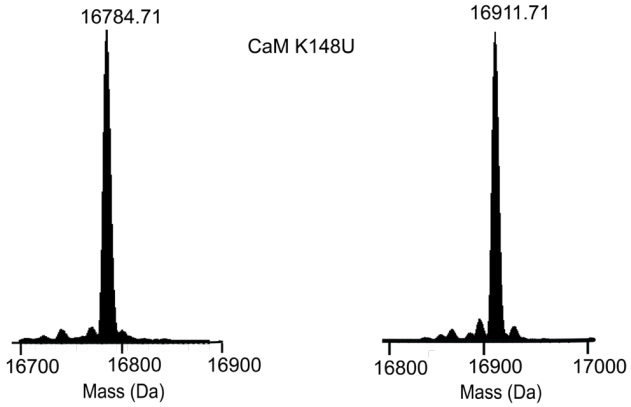

Figure S4. Deconvoluted intact protein mass spectra of calmodulin K148U. Left panel: before reaction with FDCP. The calculated mass is 16785.30 Da. Right panel: after the reaction. The reaction was carried out at 25 °C for 10 minutes. The expected mass increase is 128 Da.

Deleted: S2

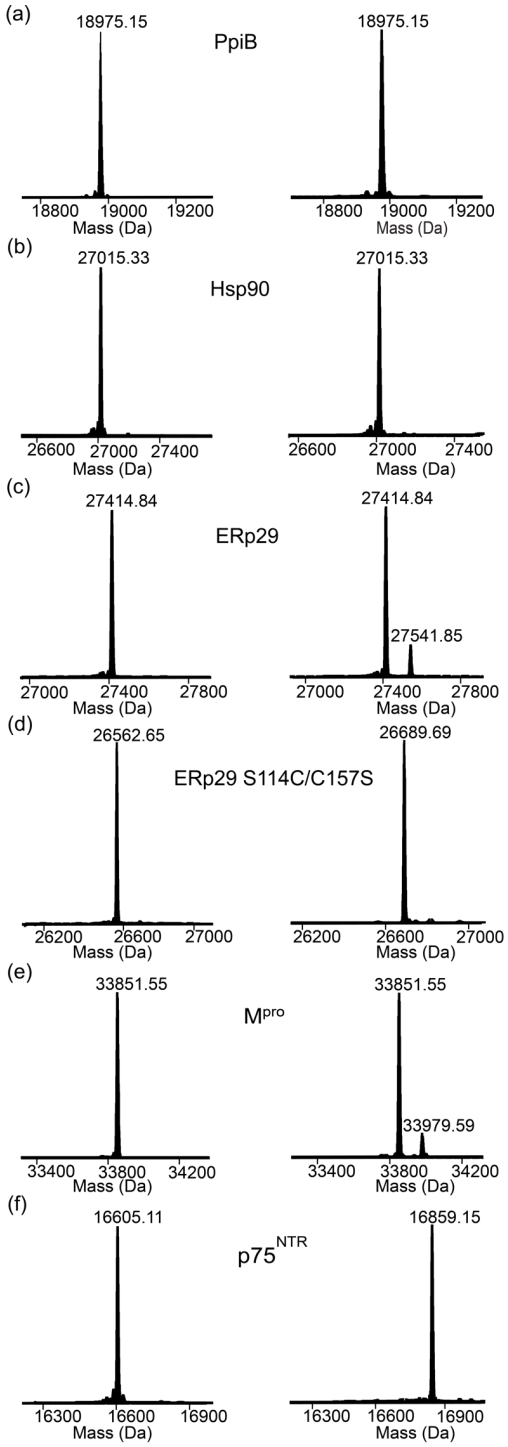
(a)
18975.15
PpiB
18975.15
18800 19000 19200
Mass (Da)
18800 19000 19200
Mass (Da)
(b)
27015.33
Hsp90
27015.33
26600 27000 27400
Mass (Da)
26600 27000 27400
Mass (Da)
(c)
27414.84
ERp29
27414.84
27541.85
27000 27400 27800
Mass (Da)
27000 27400 27800
Mass (Da)
(d)
26562.65
ERp29 S114C/C157S
26689.69
26200 26600 27000
Mass (Da)
26200 26600 27000
Mass (Da)
(e)
33851.55
Mpro
33851.55
33979.59
33400 33800 34200
Mass (Da)
33400 33800 34200
Mass (Da)
(f)
16605.11
p75NTR
16859.15
16300 16600 16900
Mass (Da)
16300 16600 16900
Mass (Da)

Figure S5. Deconvoluted intact protein mass spectra illustrating the reactivity of the FDCP tag with cysteine residues of different solvent exposure. The spectra in the left and right panels show the whole-protein mass spectra before and after reaction with the tag, respectively. The expected mass increase upon addition of a single DCP tag is 128 Da. (a) *E. coli* PpiB. The protein contains two buried cysteine residues. The calculated mass of the untagged protein is 18976.32 Da. (b) N-terminal domain of *P. falciparum* Hsp90. The protein contains a single cysteine residue with limited solvent exposure. Calculated mass (without tag): 27016.40 Da. (c) Rat ERp29. The protein contains a single cysteine residue with partial solvent exposure. Calculated mass (without tag): 27415.20 Da. (d) Rat ERp29 G147C/C157S. The protein contains one highly solvent-exposed cysteine residue. Calculated mass (without tag): 26563.28 Da. (e) SARS-2 main protease (M^{pro}). The protein contains 12 cysteine residues, three of which are partially solvent exposed (including the active-site residue C145). Calculated mass (without tag): 33851.55 Da. (f) Intracellular domain of $p75^{NTR}$. The protein contains two highly solvent-exposed cysteine residues. Calculated mass (without tag): 16606.23 Da.

Deleted: S3

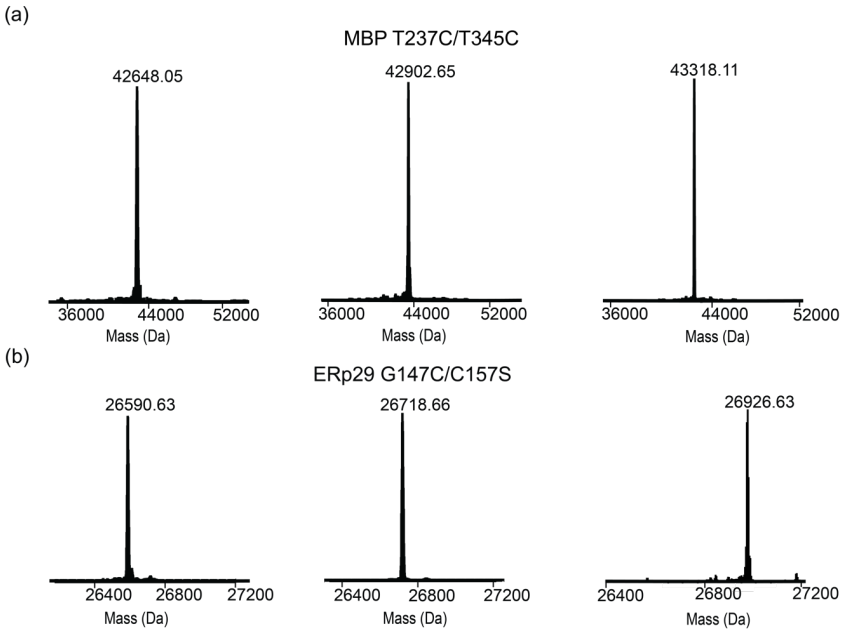

Figure S6. Deconvoluted intact protein mass spectra showing the reaction of the FDCP tag with cysteine residues in the protein (expected mass increase per DCP tag is 128 Da) and subsequent reaction of each DCP tag with two cysteine molecules (expected mass increase per DCP tag is 208 Da). Left panel: before reaction with the tag. Calculated masses are 42648.53 and 26591.96 Da respectively. Centre panel: after reaction with the FDCP tag. Right panel: after reaction with excess free cysteine to complete the metal binding tag. (a) MBP T237C/T345C. (b) ERp29 G147C/C157S.

Deleted: S4

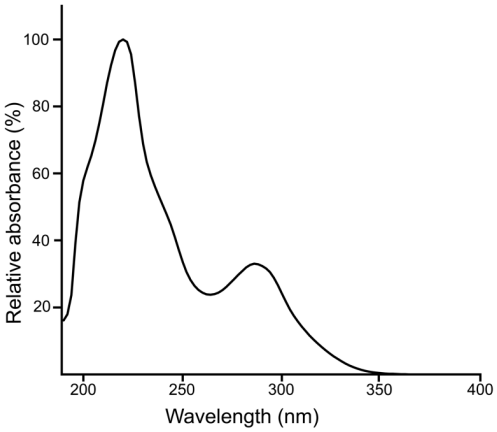

Figure S7. UV/Vis absorption spectrum of DCP-(L-Cys)$_2$. The spectrum was recorded of the DCP-(L-Cys)$_2$ fraction during a HPLC-MS run, using an Agilent mass spectrometer equipped with a reverse-phase column, a gradient from 5 % MeOH:water to 90 % MeOH:water in the presence of 0.1 % TFA and a temperature of 30 °C. Using a separate sample of DCP reacted with excess L-cysteine, the molar extinction coefficient ε at 280 nm was determined to be 6850 M^{-1} cm^{-1}. A sample of DCP reacted in the same way with excess L-penicillamine yielded ε_{280} = 5400 M^{-1} cm^{-1}.

Deleted: S5

Table S1. PCSs of backbone amide protons generated with $TbCl_3$ and $TmCl_3$ in GB1 Q32C with DCP-$(Cys)_2$ tags of different chirality.

GB1-DCP-(L-Cys)$_2$				GB1-DCP-(D-Cys)$_2$			
Tb^{3+}		Tm^{3+}		Tb^{3+}		Tm^{3+}	
Residue	PCS^{exp}/ppm	Residue	PCS^{exp}/ppm	Residue	PCS^{exp}/ppm	Residue	PCS^{exp}/ppm
Thr2	0.500	Tyr3	0.420	Thr2	-0.233	Thr2	0.118
Lys4	0.726	Lys4	0.329	Tyr3	-0.408	Tyr3	0.198
Leu5	0.905	Leu5	0.442	Lys4	-0.291	Lys4	0.147
Ile6	0.538	Ile6	0.298	Leu5	-0.423	Leu5	0.188
Leu7	0.489	Leu7	0.302	Ile6	-0.325	Ile6	0.145
Asn8	0.188	Asn8	0.162	Leu7	-0.374	Leu7	0.153
Gly9	0.093	Gly9	0.125	Asn8	-0.297	Asn8	0.115
Gly14	0.350	Gly14	0.248	Gly9	-0.285	Gly9	0.104
Glu15	0.727	Glu15	0.408	Lys10	-0.202	Lys10	0.049
Val21	1.469	Thr16	0.517	Thr11	-0.207	Thr11	0.065
Asp22	1.221	Thr18	0.423	Leu12	-0.267	Leu12	0.091
Ala23	0.713	Ala20	0.671	Lys13	-0.274	Lys13	0.102
Thr44	0.205	Val21	1.091	Gly14	-0.334	Gly14	0.129
Tyr45	0.246	Ala26	1.025	Thr16	-0.443	Thr16	0.193
Asp46	0.380	Glu27	0.697	Thr17	-0.296	Thr17	0.143
Asp47	0.308	Lys28	0.694	Thr18	-0.464	Thr18	0.210
Ala48	0.286	Thr44	0.117	Ala20	-0.605	Ala20	0.316
Thr49	0.319	Tyr45	0.109	Val21	-0.638	Val21	0.448
Lys50	0.409	Asp46	0.167	Thr25	-0.227	Thr25	0.113
Thr51	0.459	Asp47	0.128	Phe30	-1.376	Phe30	0.540
Thr53	0.348	Ala48	0.118	Thr44	-0.103	Thr44	0.048
Val54	0.274	Thr49	0.137	Thr49	-0.090	Asp46	0.060
Thr55	0.056	Lys50	0.175	Asp46	-0.097	Thr49	0.045
		Thr51	0.202	Lys50	-0.108	Lys50	0.067
		Phe52	0.300	Thr51	-0.140	Thr51	0.078
		Thr53	0.180	Thr53	-0.176	Thr53	0.083
		Val54	0.197	Val54	-0.293	Val54	0.118
		Thr55	0.076	Thr55	-0.171	Thr55	0.055
				Glu56	-0.204	Glu56	0.109

Table S2. PCSs of backbone amide protons generated with $TbCl_3$ and $TmCl_3$ in GB1 Q32C with DCP tags reacted with penicillamines of different chirality.

GB1-DCP-(L-pen)$_2$				GB1-FDCP-(D-pen)$_2$			
Tb^{3+}		Tm^{3+}		Tb^{3+}		Tm^{3+}	
Residue	PCS^{exp}/ppm	Residue	PCS^{exp}/ppm	Residue	PCS^{exp}/ppm	Residue	PCS^{exp}/ppm
Met1	1.622	Met1	-0.787	Thr2	-0.856	Thr2	0.478
Thr2	1.033	Thr2	-0.519	Lys4	-0.845	Lys4	0.471
Tyr3	1.505	Tyr3	-0.748	Leu5	-1.065	Leu5	0.570
Lys4	0.935	Lys4	-0.455	Ile6	-0.696	Ile6	0.347
Ile6	0.429	Ile6	-0.220	Leu7	-0.686	Leu7	0.328
Leu7	0.289	Leu7	-0.197	Asn8	-0.507	Asn8	0.223
Glu15	0.387	Glu15	-0.281	Gly9	-0.432	Gly9	0.180
Thr18	1.436	Thr18	-0.752	Lys10	-0.297	Lys10	0.122
Gly41	-0.409	Thr25	-0.505	Thr11	-0.279	Thr11	0.120
Trp43	-0.250	Gly41	0.199	Leu12	-0.351	Leu12	0.137
Tyr45	0.159	Trp43	0.127	Lys13	-0.401	Lys13	0.155
Asp46	0.398	Asp46	-0.162	Gly14	-0.566	Gly14	0.249
Asp47	0.345	Asp47	-0.521	Glu15	-0.728	Glu15	0.331
Ala48	0.352	Ala48	-0.153	Thr16	-1.052	Thr16	0.516
Thr49	0.407	Thr49	-0.186	Thr18	-1.504	Thr25	0.421
Lys50	0.554	Lys50	-0.254	Thr25	-0.771	Gly41	0.117
Thr51	0.554	Thr51	-0.254	Gly41	-0.337	Asp46	0.145
Phe52	0.650	Phe52	-0.300	Asp46	-0.218	Asp47	0.074
Thr53	0.235	Thr53	-0.101	Asp47	-0.068	Ala48	0.099
				Ala48	-0.118	Thr49	0.137
				Thr49	-0.221	Lys50	0.188
				Lys50	-0.276	Thr51	0.219
				Thr51	-0.358	Phe52	0.350
				Phe52	-0.633	Thr53	0.188
				Thr53	-0.350	Glu56	0.129
				Val54	-0.529		
				Thr55	-0.190		
				Glu56	-0.315		

Table S3. $^{1}D_{HN}$ RDCs of backbone amides of GB1 Q32C with different DCP tags loaded with Tb^{3+} ions.

DCP-(D-pen)$_2$-Tb		DCP-(L-Cys)$_2$-Tb	
Residue	RDC/Hz	Residue	RDC/Hz
Thr2	11.1	Thr2	-6.6
Leu5	-11.3	Lys4	-6.8
Ile6	-18.7	Leu5	5.7
Leu7	-9.5	Ile6	2.0
Asn8	-11.1	Leu7	5.6
Gly9	-5.7	Asn8	3.9
Lys10	5.3	Gly9	6.7
Thr11	2.0	Lys10	2.3
Leu12	-8.0	Gly14	0.2
Lys13	-14.6	Glu15	-6.2
Gly14	-12.1	Val21	2.0
Glu15	-13.4	Thr44	8.3
Thr16	-17.5	Tyr45	-1.1
Thr25	-2.3	Asp46	4.8
Gly41	10.0	Ala48	9.2
Asp46	-13.3	Thr49	-1.0
Asp47	-10.0	Lys50	-5.6
Ala48	1.5	Thr51	-0.1
Thr49	6.0	Phe52	5.1
Lys50	-14.3	Thr53	5.1
Thr51	-9.2	Thr55	5.1
Phe52	-12.5		
Thr53	-13.9		
Val54	-9.9		
Thr55	-9.9		
Glu56	-2.9		

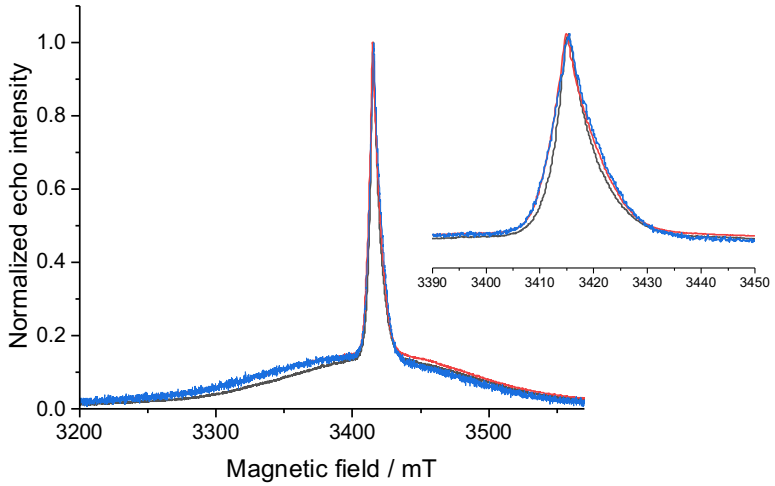

Figure S8. Echo-detected W-band EPR spectra of ERp29 S114/C157S DCP-(β-Cys)$_2$-Gd (black), MBP T237U/T345U DCP-(L-Cys)$_2$-Gd (red) and MBP T237C/T345C DCP-(L-Cys)$_2$-Gd (blue). All samples targeted a metal-to-tag ratio of 1:1 but contained about 20 % excess of Gd^{3+} ions because the protein concentration was overestimated due to neglecting the contribution of the tag to the absorbance at 280 nm.

Deleted: S6

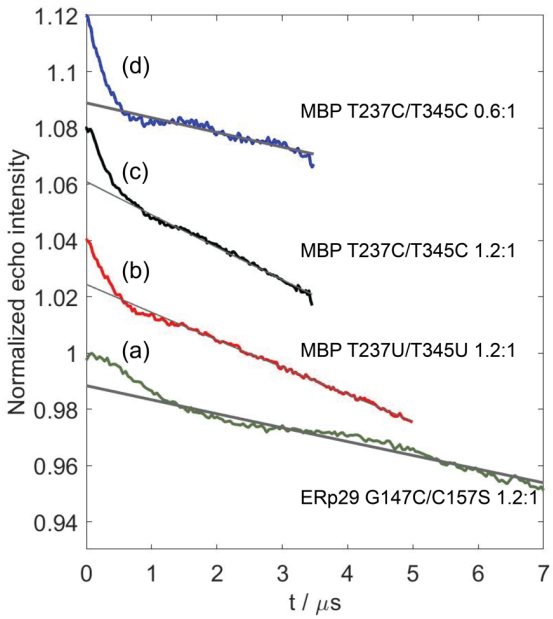

Figure S9. Primary DEER traces of Fig. 4 in the main text. The background decay is shown as grey lines. (a) ERp29 G147C/C157S with 1.2:1 metal-to-tag ratio. (b) MBP T237U/T345U with a metal-to-tag ratio of 1.2:1. (c) MBP T237C/T345C with a metal-to-tag ratio of 1.2:1. (d) Same as (c), but with a metal-to-tag ratio of 0.6:1.

Deleted: ¶
¶
Deleted: S7

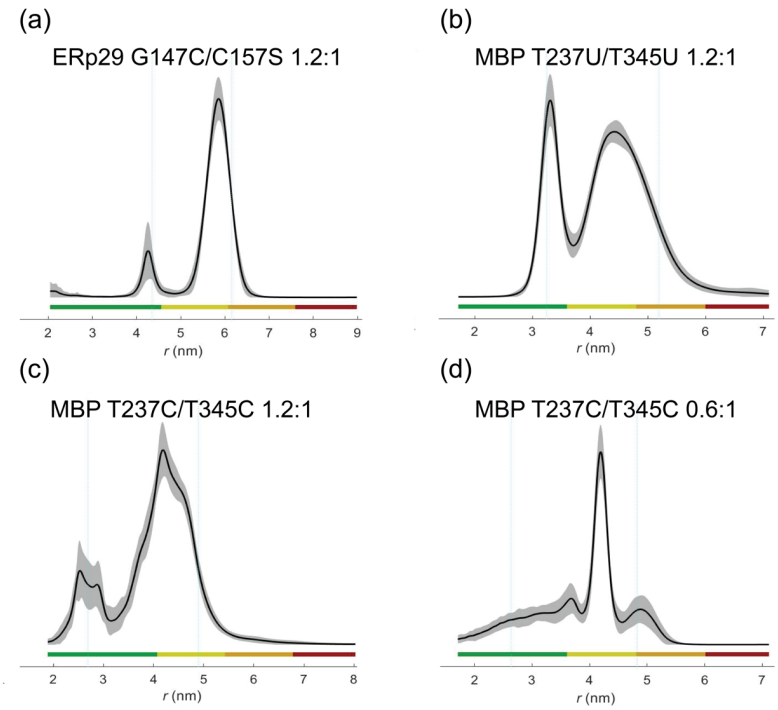

Figure S10. Distance distributions of Fig. 4 analysed by DeerNet as implemented in DeerAnalysis2022 (Worswick et al., 2018), with colour coding of the reliability regions as defined in DeerAnalysis (Jeschke et al., 2006), corresponding to the DEER evolution time used (green: the shape of the distance distribution is reliable. Yellow: the mean distance and distribution width are reliable. Orange: the mean distance is reliable. Red: long-range distance contributions may be detectable but cannot be quantified). The solid lines represent the distributions with the best r.m.s.d. from the experimental data and the striped regions represent the variation of alternative distributions (±2 times the standard deviation) obtained by varying the parameters of the background correction and noise as calculated by the validation tool in the DeerAnalysis software package. The parameter ranges used for the validations were the default ones: white noise 0–1.5, background start $0.2*t_{max}$–$0.6*t_{max}$, and background dimension 3–3.6.

Deleted: S8

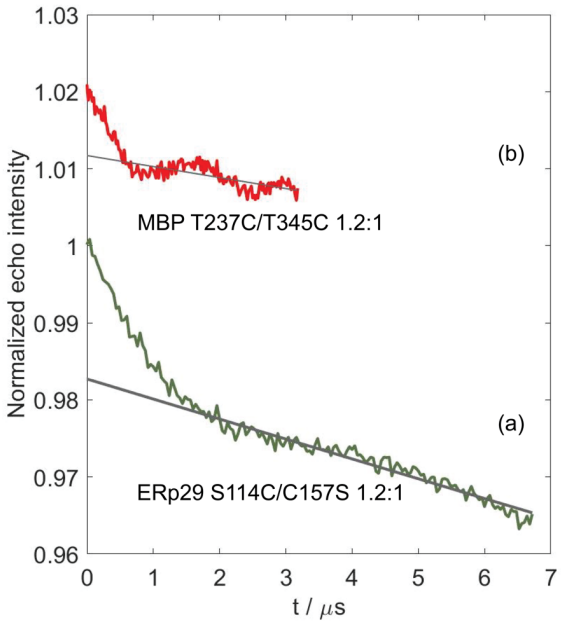

Figure S11. Raw DEER traces of Fig. 5 in the main text. The background decay is shown as grey lines. (a) ERp29 S114C/C157S. (b) MBP T237C/T345C.

Deleted: S9

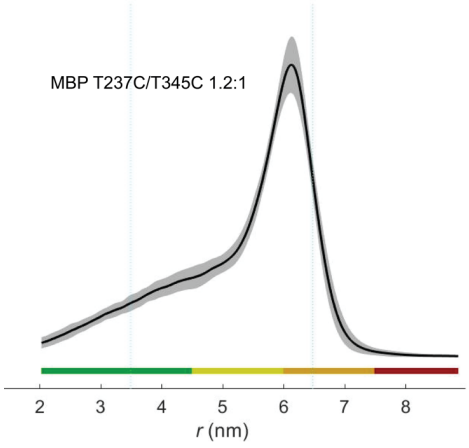

Figure S12. Distance distribution of MBP T237C/T345C (Fig. 5 of the main text) analysed by DeerNet (Worswick et al., 2018) with colour coding of the reliability regions as defined in Fig. S10.

Deleted: S10

Deleted: 8

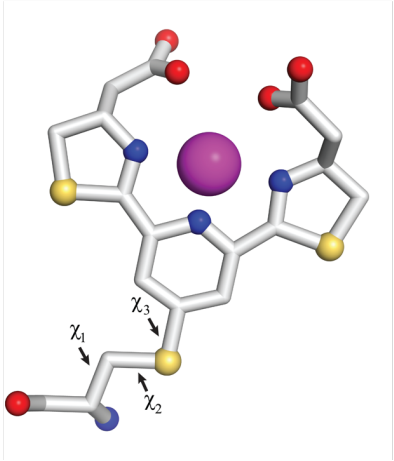

Figure S13. Conformation of the DCP-(β-Cys)$_2$-Gd tag attached to cysteine as used for modelling distance distributions. Dihedral angles χ of rotatable bonds are labelled. Blue, red, yellow and magenta balls identify atoms of nitrogen, oxygen, sulfur and gadolinium, respectively. The conformation was modelled using ChemDraw, which placed the metal ion 1.9 Å from the pyridine nitrogen and 2.3 Å from the thiazoline nitrogens.

Deleted: S11

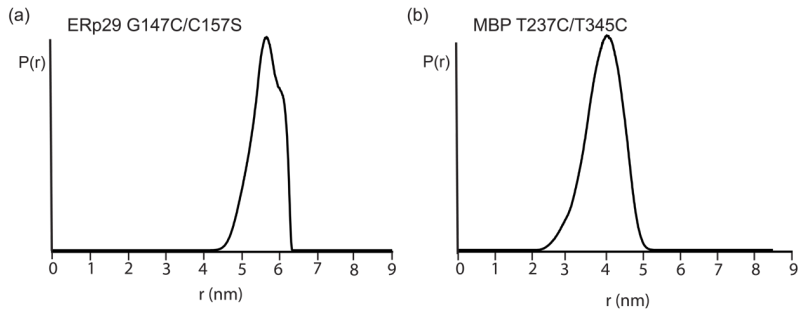

Figure S14. Gd^{3+}–Gd^{3+} distance distributions calculated with the program PyParaTools (Stanton-Cook et al., 2014) using rotamer libraries of the DCP-Cys_2-Gd tag bound to cysteine, generated by varying the χ_1 angle by ±30° around the staggered rotamers and allowing free rotation about the χ_2 and χ_3 angles. (a) ERp29 G147C/C157S. (b) MBP T237C/T345C.

Deleted: S12

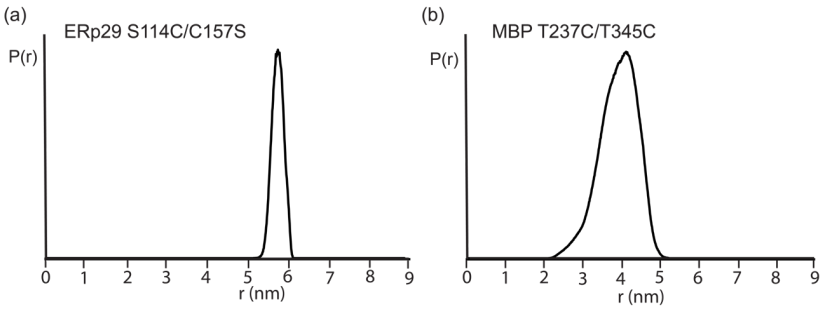

Figure S15. Gd^{3+}–Gd^{3+} distance distributions calculated with the program PyParaTools using rotamer libraries of the DCP-$(\beta\text{-Cys})_2$-Gd tag bound to cysteine (see Fig. S12), generated by varying the χ_1 angle by ±30° around the staggered rotamers and allowing free rotation about the χ_2 and χ_3 angles. (a) ERp29 S114C/C157S. (b) MBP T237C/T345.

Deleted: S13

Deleted: 6

Deleted: ¶

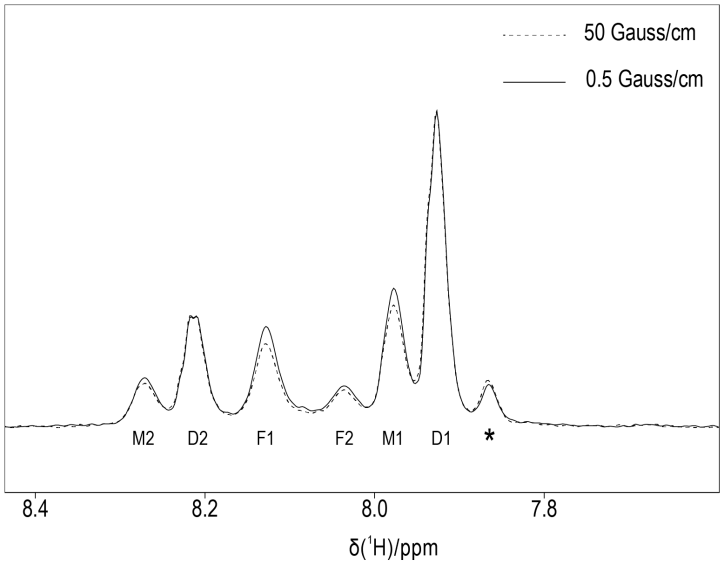

Figure S16. Diffusion experiment of DCP-(L-Cys)$_2$ in the presence of YCl_3. The spectrum was recorded of a 0.3 mM solution of DCP-(L-Cys)$_2$ in 10 mM HEPES buffer (pH 7) in D_2O with 0.5 equivalents of YCl_3, using a 800 MHz NMR spectrometer. The pulse sequence used a stimulated echo with bipolar gradients (Bruker pulse program stebpggp1s191d). Each pulsed field gradient was 2 ms and the duration of the diffusion delay Δ was limited to 10 ms to prevent chemical exchange from equilibrating the peak intensities. The spectra plotted with solid and dashed lines were recorded with weak (0.5 Gauss/cm) and strong (50 Gauss/cm) gradients, the latter resulting in about 11-fold signal attenuation. The loss in sensitivity was compensated by recording the attenuated spectrum with 8192 instead of 1024 scans. Scaling of the peaks D1 and D2 for closest superimposition, the signals of the free ligand (F1 and F2) and the 1:1 complex (M1 and M2) are smaller with strong than weak gradients, indicating more rapid diffusion as expected, if D1 and D2 correspond to the 2:1 ligand-to-protein complex. The signal labelled with a star showed no exchange cross-peaks (Fig. S17) and is unassigned. A corresponding diffusion experiment conducted with GB1 Q32C tagged with DCP-(L-Cys)$_2$ and titrated with 0.6 equivalents $TmCl_3$ yielded no measurable difference in peak attenuation between diamagnetic and paramagnetic signals.

Formatted: Font: 10 pt

Formatted: Font: Symbol

Formatted: Not Superscript/ Subscript

Formatted: Subscript

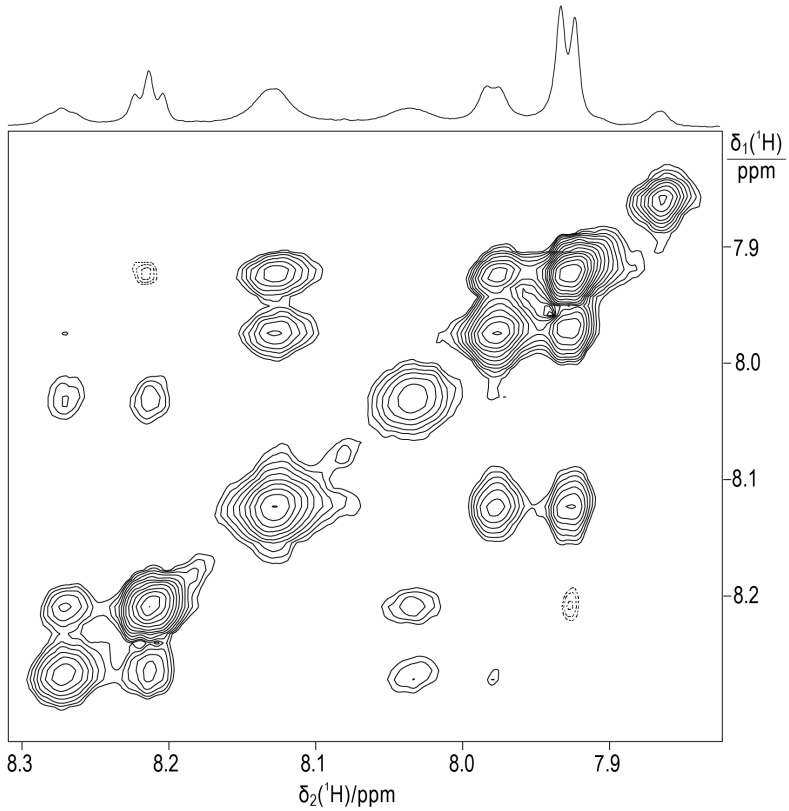

Figure S17. EXCSY spectrum of DCP-(L-Cys)$_2$ in the presence of YCl_3. The spectrum was recorded of the sample used to record the data of Fig. S16. The 1D NMR spectrum (see Fig. 6 of the main text) is shown at the top. The spectrum was recorded at 800 MHz with a mixing time of 25 ms, t_{1max} = 40 ms, t_{2max} = 160 ms. Negative contour levels associated with zero-quantum cross-peaks are plotted with dashed lines. Dividing the cross-peak intensities by the diagonal intensities and the mixing time yields an exchange rate between free and bound metal ion of about 10 s^{-1}.

Table S4. Nucleotide sequences of the genes of ERp29 with TEV site preceding a C-terminal His_6 tag, GB1 preceded by a MASMTG tag and followed by a TEV site and C-terminal His_6 tag, and list of mutation primers used.

Protein	DNA Sequence	Primers
ERp29_TEV_C-His_6	ATGCTGCACACGAAGGGCGCCCTTCCCTTGGA CACAGTCACTTTCTACAAGGTCATTCCCAAAAG CAAGTTCGTCTTGGTGAAGTTCGACACCCAGTA CCCCTATGGAGAGAAGCAAGATGAGTTTAAGC GTCTGGCTGAGAACTCAGCCTCCAGCGATGAT CTCTTGGTGGCAGAGGTGGGGATCTCAGACTA TGGTGACAAGCTGAACATGGAGCTGAGTGAGA AGTACAAGCTGGACAAAGAGTCTTACCCAGTC TTCTACCTCTTCCGGGATGGGGACTTTGAGAAT CCTGTCCCATACAGCGGGGCAGTTAAAGTTGG AGCCATCCAGCGCTGGCTCAAGGGGCAGGGAG TCTATCTGGGCATGCCTGGATGTCTGCCTGCGT ACGATGCCCTGGCGGGCCAGTTCATCGAGGCC TCCAGCAGAGAGGCCCGCCAGGCCATCCTGAA ACAGGGGCAGGATGGCCTCTCAGGTGTGAAGG AGACAGACAAGAAGTGGGCCAGTCAGTACCTG AAGATCATGGGGAAGATCTTGGACCAAGGTGA AGACTTCCCGGCCTCCGAGCTGGCCCGGATCA GTAAGCTCATTGAGAACAAGATGAGTGAGGGT AAGAAGGAAGAGCTGCAGAGGAGCCTCAACA TCCTCACCGCCTTCCGCAAGAAAGGCGCCGAG AAGGAGGAGCTCGAAAACCTGTATTTTCAGGG CCACCATCACCATCACCATTA	Forward primer (for amplifying the pETMCSI backbone): GAATTCGAGCTCCCGGGTAC Reverse primer (for amplifying the pETMCSI backbone): CATATGTATATCTCCTTCTTA AAGTTAAAC. Forward primer (for amplifying the ERp29_TEV_C-His_6 gene): GTTTAACTTTAAGAAGGAGA TATACATATGCTGCACACGA AG Reverse primer (for amplifying the ERp29_TEV_C-His_6 gene): GTACCCGGGAGCTCGAATTC TTAATGGTGATGGTGATG
MASMTG_GB1_TEV_C-His_6	ATGGCTTCTATGACCGGTATGACCTACAAACTG ATCCTGAACGGTAAAACCCTGAAAGGTGAAAC CACCACCGAAGCGGTTGACGCGGCGACCGCGG AAAAAGTTTTCAAACAGTACGCGAACGACAAC GGTGTTGACGGTGAATGGACCTACGACGACGC GACCAAAACCTTCACCGTTACCGAAGAAAACC TGTATTTTCAGGGCCACCATCACCATCACCAT	Forward primer (for Q32C mutation): GTTTTCAAATGCTACGCGAA CGACAACGGTGTTG Reverse primer (for Q32C mutation): GCGTAGACTTTGAAAACTTT TTCCGCGGTCGCCG

Formatted: Font:

References

Bergeron, R. J., Wiegand, J., Weimar, W. R., Vinson, J. R. T., Bussenius, J., Yao, G. W., and McManis, J. S.: Desazadesmethyldesferrithiocin analogues as orally effective iron chelators, J. Med. Chem., 42, 95–108, https://doi.org/10.1021/jm980340j, 1998.

Birkofer, L. and Birkofer, A.: β-Aminosäuren, VII. Mitteil.: β-Homocystein, Chem. Ber.-Recueil, 89, 1226–1229, https://doi.org/10.1002/cber.19560890522, 1956.

Jeschke, G., Chechik, V., Ionita, P., Godt, A., Zimmermann, H., Banham, J., Timmel, C., Hilger, D., and Jung, H.: DeerAnalysis2006–a comprehensive software package for analyzing pulsed ELDOR data, Appl. Magn. Reson., 30, 473–498, https://doi.org/10.1007/BF03166213, 2006.

Kim, B. C., Kim, K. Y., Lee, H. B., An, J. E., and Lee, K. W.: Production method of intermediate compound for synthesizing medicament, US Patent US8741927B2, 2014.

Stanton-Cook, M. J., Su, X.-C., Otting, G., and Huber, T.: PyParaTools, available at http://comp-bio.anu.edu.au/mscook/PPT/ (last access: 1 May 2022), 2014.

Worswick, S. G., Spencer, J. A., Jeschke, G., and Kuprov, I.: Deep neural network processing of DEER data, Sci. Adv., 4, eaat5218, https://doi.org/10.1126/sciadv.aat5218, 2018.

Formatted: Font: (Default) Times New Roman
Formatted: Justified
Formatted: Font: Times New Roman, 12 pt
Formatted: Font: Times New Roman, 12 pt
Formatted: Line spacing: 1.5 lines
Formatted: Font: Symbol
Formatted: Font: Symbol
Formatted: Font: Times New Roman, 12 pt
Formatted: Normal, Justified, Indent: Left: 0 cm, Line spacing: 1.5 lines
Formatted: Font colour: Text 1, English (AUS)